UCRL-18654
cy. 2

RECEIVED
LAWRENCE
RADIATION LABORATORY
1969
LIBRARY AND
DOCUMENTS SECTION

PIONIC ATOMS

Arthur Raymond Kunselman
(Ph. D. Thesis)

April 1969

TWO-WEEK LOAN COPY

This is a Library Circulating Copy which may be borrowed for two weeks. For a personal retention copy, call Tech. Info. Division, Ext. 5545

LAWRENCE RADIATION LABORATORY
UNIVERSITY of CALIFORNIA BERKELEY

UCRL-18654
cy. 2

DISCLAIMER

This document was prepared as an account of work sponsored by the United States Government. While this document is believed to contain correct information, neither the United States Government nor any agency thereof, nor the Regents of the University of California, nor any of their employees, makes any warranty, express or implied, or assumes any legal responsibility for the accuracy, completeness, or usefulness of any information, apparatus, product, or process disclosed, or represents that its use would not infringe privately owned rights. Reference herein to any specific commercial product, process, or service by its trade name, trademark, manufacturer, or otherwise, does not necessarily constitute or imply its endorsement, recommendation, or favoring by the United States Government or any agency thereof, or the Regents of the University of California. The views and opinions of authors expressed herein do not necessarily state or reflect those of the United States Government or any agency thereof or the Regents of the University of California.

PIONIC ATOMS

Table of Contents

Abstract v

I. Introduction 1

A. Interest of Studies. 1

B. Historical Survey. 4

II. Experimental Setup 6

A. Beam 6

B. Counters and Geometry. 8

C. Electronic Logic 10

D. Germanium Spectrometers. 12

E. Targets. 17

F. Calibration. 20

III. Strong-Interaction Line Shifts and Widths. 25

A. Computation of Pionic X-ray Energies 25

B. Computation of Pionic X-ray Line Widths. 27

C. Experimental Measurements. 27

D. Phenomenological Pion-Nuclear Optical Model. 37

E. Comparison of Theory and Experiment. 48

IV. X-ray Yields of the Elements 50

A. Method and Results 50

V. Line Intensities in Compounds 65

A. Chemical Effects. 65

B. Chlorides 72

Acknowledgments 76

Appendix. 77

References. 81

PIONIC ATOMS

Arthur Raymond Kunselman

Lawrence Radiation Laboratory
University of California
Berkeley, California

ABSTRACT

We measured the X rays produced by negative pions stopped in various targets. We measured the line shifts, line widths, and line intensities in pure element targets to observe the effect of the pion-nuclear strong interaction. We present an optical model analysis for the shifts and widths. We measured the line intensities in chemical compound targets to observe the effects of the chemical composition of the target on the pion capture probability by the constituents. We used germanium solid state detectors throughout.

I. INTRODUCTION

A. Interest of Studies

A pion can be brought to rest in matter in a time short compared to the pion lifetime. A pionic atom forms when an atom captures a negative pion into an orbit. The initial orbit will usually be among the valence electrons and will have a large principal quantum number. The pion cascades down in a time of the order of 10^{-12} sec by means of Auger electron ejection and radiation emission. We observe the X rays from the transitions during the last stages of the cascade. The nucleus eventually captures the pion because of the overlap of the pion wave function with the nucleus. The influence of the nucleus by means of the strong interaction appears in the last orbits before capture.

The pionic X rays will be 273 times more energetic than electronic X rays for the corresponding transitions because of the larger pion mass m_π,

$$E(n_1 \rightarrow n_2) = \frac{m_\pi Z^2 e^4}{2\hbar^2} \left(\frac{1}{n_1^2} - \frac{1}{n_2^2}\right) . \qquad \text{(I-1)}$$

The pion orbits will be 273 times smaller than the corresponding electron orbits because of the larger pion mass,

$$r = a_o \frac{n^2}{Z} \left(\frac{m_e}{m_\pi}\right) , \quad \text{where} \quad a_o = \frac{\hbar^2}{m_e e^2} . \qquad \text{(I-2)}$$

Using a Bohr orbit for the single pion one finds the pion will be inside the K-shell electrons at n=16 independent of Z. Using a uniform density nucleus one finds the pion will be on the nuclear surface at n=1 for Z=35.

The pion-nuclear interaction affects the n=1 orbit for all Z greater than 3. The orbital velocity for the electron and for the pion is independent of mass, $v = \frac{Z}{n} \alpha c$, so relativistic effects are equally influential in both electron and pionic atoms.

The X-ray properties that we measure are energy shifts, line widths, and transition yields. The pionic X rays are interesting in two respects; we will deduce the pion-nuclear interaction parameters, and the initial atomic capture probabilities. Recent developments of solid state detectors produced improved resolution over previous methods of measurement with scintillation counters and proportional counters. A large number of transition energies fall into the energy range having a favorable efficiency using a germanium detector.

We stopped the negative pion beam in various target materials and observed the X rays which were produced. We calibrated the detector with radioactive gamma ray sources so that we knew the energy of observed X-ray lines. We calculated, as explained in detail later, the purely electromagnetic energy of pionic X rays. We attributed any difference between the measured and calculated X-ray energies to a shift resulting from the presence of the pion-nuclear interaction.

A pionic X-ray line may be broader than a calibration line from a radioactive source or muonic atom X ray indicating a true intrinsic width. We attribute this width of the line to the strong pion-nuclear interaction, primarily the pion absorption by the nucleus, which shortens the life of the lower state and thus broadens the line. Nuclear capture in the upper state may also reduce the X-ray line intensity from that to be expected from the electromagnetic transition probablility.

The chemical state of the atom which captures the pion can affect the intensity of a particular X-ray line. This chemical effect is not well understood but we compare the pionic atom experimental results with muonic atom results. The technique is to observe the intensity of pionic X-ray lines and deduce the fraction of pions captured on the various kinds of atoms of a compound, alloy, or mixture. We will discuss the factors that influence the measured ratios.

B. Historical Survey

Yukawa predicted in 1935 the pion to exist as the quantum of the nuclear force field.[1] Powell et al. in 1947 discovered the pion in cosmic radiation from observation of a disintegration star after nuclear capture in emulsion.[2] Fermi et al. suggested the possible existence of mesic atoms in 1947.[3] Fermi and Teller in 1947 calculated a time of about 10^{-13} sec for a π^- to reach the K-shell.[4] The cascade time of 10^{-13} sec was short compared to the pion lifetime of 2.6×10^{-8} sec. Camac et al. in 1952 first observed pionic X rays.[5] They used a scintillation counter and a carbon target.

An early result was the observation of the pion-nuclear shift of the X-ray line and determination of the repulsive interaction between an s-wave pion and a nucleon.[6] West wrote in 1957 a survey article of the earlier measurements.[7] Experimenters (using a bent crystal spectrometer) measured the mass of the pion with pionic X rays at Berkeley in 1965.[8] Improvements in measurement, possible with solid state detectors, encouraged recent interest. Ericson and Ericson[9] considered details of the theory of the pion-nuclear interaction. They derived a pion-nuclear optical potential from multiple scattering theory and determined parameters in the potential from πN (pion-nucleon) scattering amplitudes and π production in NN scattering. From our measurements at Berkeley we investigated the pion-nuclear optical potential and compared it to that predicted by the Ericsons.

Recent high resolution studies include work performed at Berkeley,[10,11,12,13] CERN,[14,15] and William and Mary[16] for the strong interaction effects, at the Joint Institute for Nuclear Research,[17,18]

Chicago,[19] CERN,[20,21] and Berkeley[22] for the chemical effects.

II. EXPERIMENTAL SETUP

A. Beam

Figure 1 shows the beam arrangement. We directed the circulating proton beam of the 184-inch cyclotron onto an internal Be target. Negative pions, muons, and electrons came out of the tank and through the first collimating quadrupole Q1. This quadrupole made the beam parallel.

After Q1 the beam passed through the meson wheel which acted as a beam collimator. Then the beam went through the bending magnet H which momentum analyzed the beam. We chose the current for H and hence the beam momentum (187 MeV/c) to give the optimum number of pions. Next came the second quadrupole Q2 which focused the beam onto the pion stopping target. This target was in the counter telescope on the counter table as shown in Fig. 2.

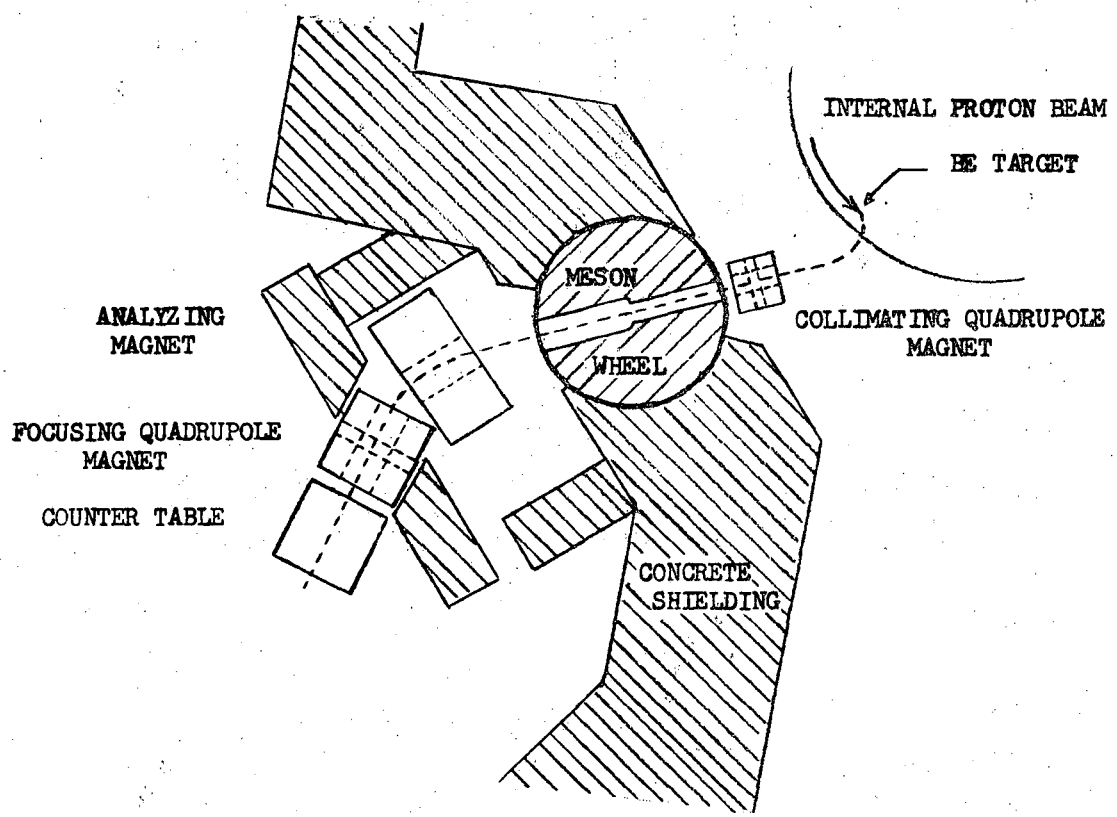

XBL 6812-6251

Fig. 1. Magnet and beam arrangement at the 184-inch cyclotron. The useful negative beam went along the dashed line. The scale is 1/2 inch to 1 meter.

B. Counters and Geometry

Figure 2 shows the counter arrangement. The counters S were plastic scintillators and the counter $\check{C}$ was a water Cerenkov counter. We monitored several counters and counter coincidences on scalers. We kept track of stopped particle defined by the coincidence $S=S_1-S_2-S_3-S_4$, beam particle defined by the coincidence $B=S_1-S_2-S_3$, stopped pion defined by the coincidence $S_\pi=S_1-S_2-S_3-\bar{S}_4-\bar{\check{C}}$, and $\check{C}$ and S_4 separately. Typical instantaneous rates for the 60% duty cycle of the stretched cyclotron beam were 3×10^5 counts sec^{-1} for S_π, and 3×10^3 counts sec^{-1} on the Ge detector (above a 30 keV threshold). The Cerenkov counter served to veto electrons in the beam and was insensitive to muons and pions.

We made S_3 of thin scintillator plastic the size of the stopping target and wrapped it carefully to avoid excess stopping material. Aluminized mylar and black tape of less than 8 mils covered the downstream face of S_3. The anti-counter S_4 was thin so as to be transparent to low energy X rays. The size of counter S_4 was sufficient to prevent scattered beam particles from escaping. We also wrapped the anti-counter carefully on the upstream face to have minimum stopping material simulating stopped pions. The position of the anti-counter was as close to the target and S_3 as possible.

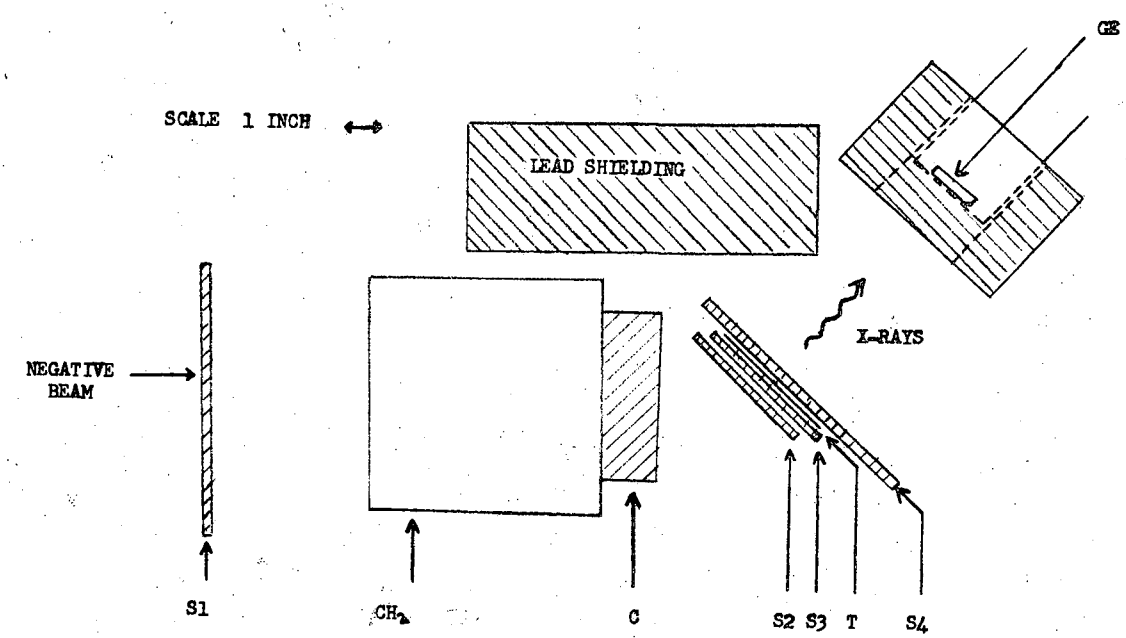

S1 1/4 x 8 x 8 plastic scintillator
S2 1/4 x 4 x 4 plastic scintillator
S3 1/16 x 4 x 4 plastic scintillator
S4 1/8 x 8 x 8 plastic scintillator
C 1-3/4 x 5 x 5 water Cerenkov counter
GE Lithium drifted germanium detector

XBL 6812-6258

Fig. 2. Counter arrangement for the stopping of pions in target T. The CH_2 material (6-1/2") in the form of sheets of polyethelene was placed in the beam to maximize the number of pions stopping in T.

C. Electronic Logic

Figure 3 shows the electronic logic diagram. We plateaued the counters. We set the gain on the output pulse of counter S_3 to eliminate some pulses from muons but not greatly affect the pulses from pions. In order to optimize the beam rate and the stopped pion rate, we also varied the magnet current settings and the internal target position.

We obtained two pulses from the linear amplifier, one slow output pulse for energy analysis and one fast output pulse for timing.[23] The timing pulse had about 50 ns rise time with variations resulting from the transit time of electrons in the Ge crystal. The coincidence timing was on the leading edge of the timing pulse. We made the coincidence between a germanium pulse and a stopped pion about 100 ns. The threshold of the coincidence at about 30 keV was well below the X-ray energy of interest. Figure 4 shows the amplifier output pulse shapes from the Ge detector, and Fig. 5 shows the amplifier electronic logic.

We put the stopped pion signal, S_π, in coincidence with the fast linear amplifier output from the Ge detector. We used this coincidence to open the linear gate and allow the pulse from the linear amplifier slow output to pass on to the pulse height analyzer. The coincidence did not cause a loss of true pulses and reduced the rate of random pulses.

We used a pile up rejector (PUR) to reject pulses which appeared within a certain set time (15 μsec) after a previous pulse. This eliminated a loss in resolution due to pulses appearing on the tail of a previous pulse.

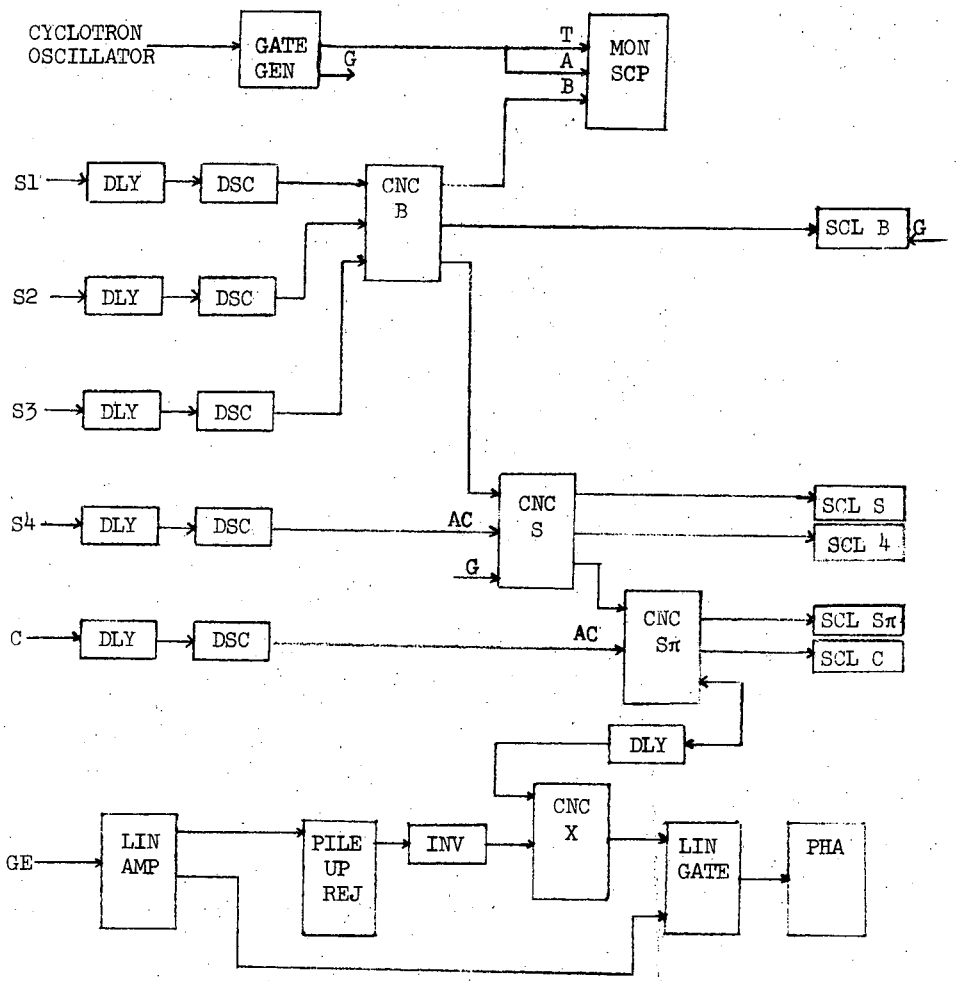

DLY	Delay
DSC	Discriminator
CNC	Coincidence
INV	Inverter
PHA	Pulse height analyzer
S	Scintillator
C	Cerenkov counter
GE	Germanium detector
G	Gating pulse
MON SCP	Monitor scope
AC	Anti-coincidence

XBL 6812-6249

Fig. 3. Electronic logic diagram.

D. Germanium Spectrometers

We placed a germanium detector (and necessary cryostat system) 15 cm from the beam line. The detector was shielded from possible beam scatters by lead and copper. The target was a sheet of material placed in the pion beam at an angle of 45°. In the early stages of the experiment the line of sight of the germanium detector was at 45° to the face of the target but in later stages of the experiment it was perpendicular to the target face. Both configurations for the detector were satisfactory but the latter had the advantage of having the same amount of material in the pion beam and less material for attenuating the X rays getting out of the target to the detector.

The detectors[13,22] were discs of 3 cm diameter and 9.5 mm drift depth. They used a bias of -2500 volts and gave a resolution of 2.2 keV (f.w.h.m.) at the 1333 keV line of ^{60}Co, and 1.3 keV at the 122 keV line of ^{57}Co.

We obtained the efficiency of the detector by placing sources of known calibrated intensity[24] at the place that would be occupied by the center of the target but without the target in position. This procedure included the absorption and scattering of the gamma rays by the anti-counter, as well as the solid angle and intrinsic efficiency of the detector. During calibration we kept the rate on the germanium detector very close to the rate of the X-ray measurements to avoid differences in dead time. We plotted the absolute efficiency of number of γ-rays measured per disintegration as a function of energy. Figure 6 shows the total efficiency to detect an X ray of a given energy. We took into account the decay scheme branching.

We also found the relative shape of the efficiency curve with sources having several known relative intensity lines.[25] The shape of the relative efficiency agreed with the absolute efficiency so that we had confidence over energy intervals with few absolute sources and over energy intervals where the shape of the efficiency curve changed. The efficiency at any energy was difficult to obtain to better than five percent precision. To check for gain drifts or efficiency changes, we frequently checked the calibration for energy and efficiency.

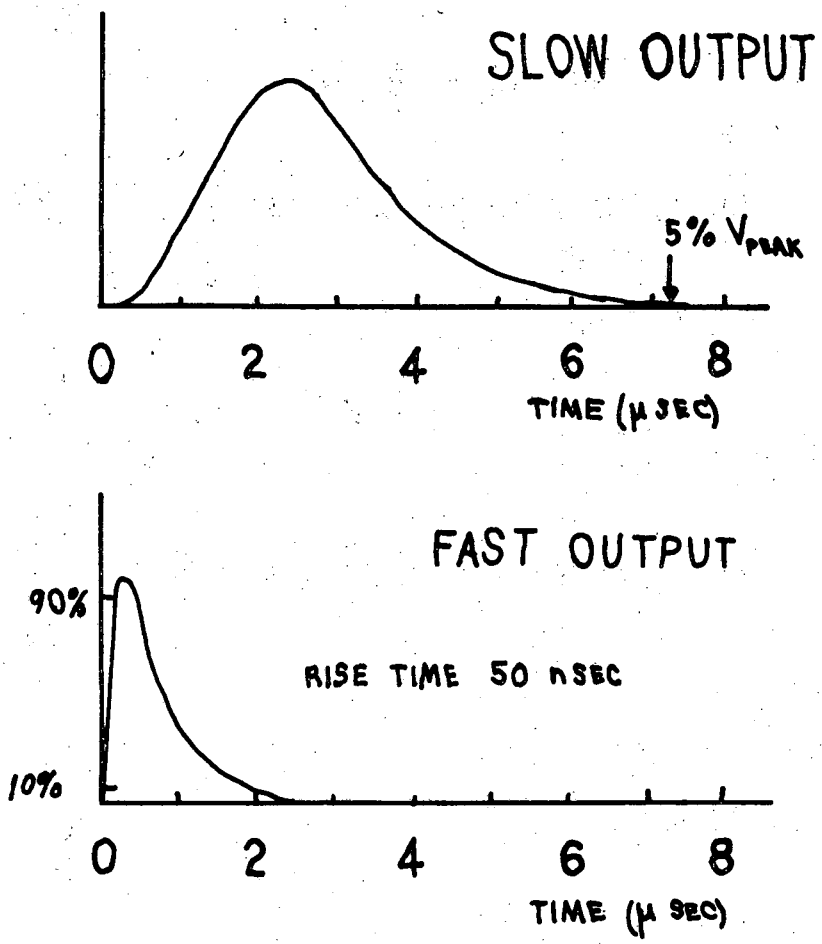

XBL 6812-6259

Fig. 4. Amplifier output pulse shapes.

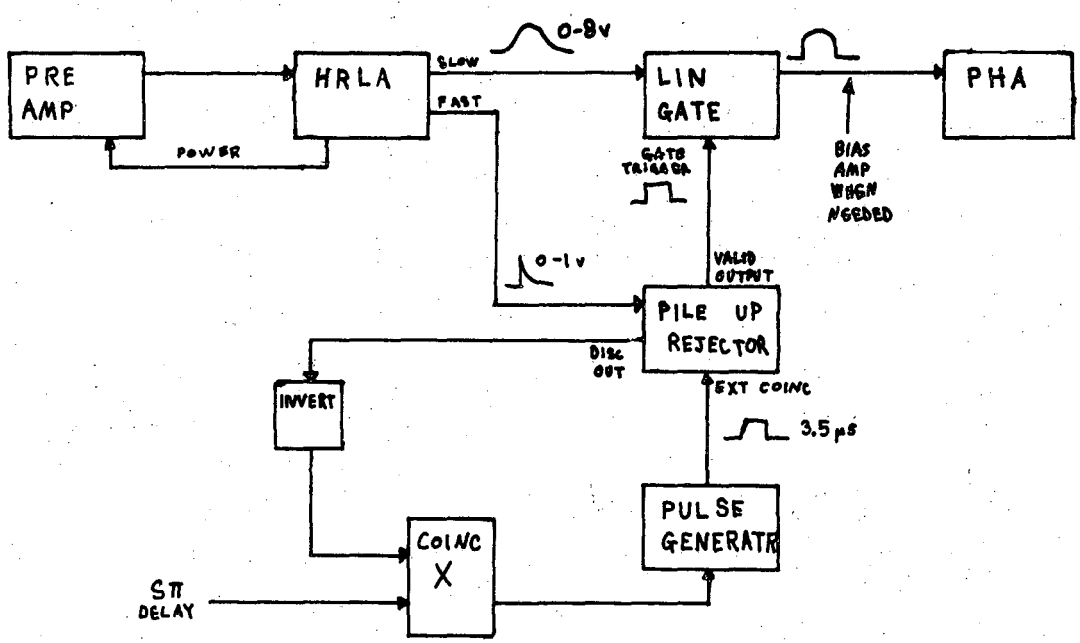

XBL 6812-6260

Fig. 5. Amplifier electronic logic. The abbreviations are HRLA-high rate linear amplifier and PHA-pulse height analyzer.

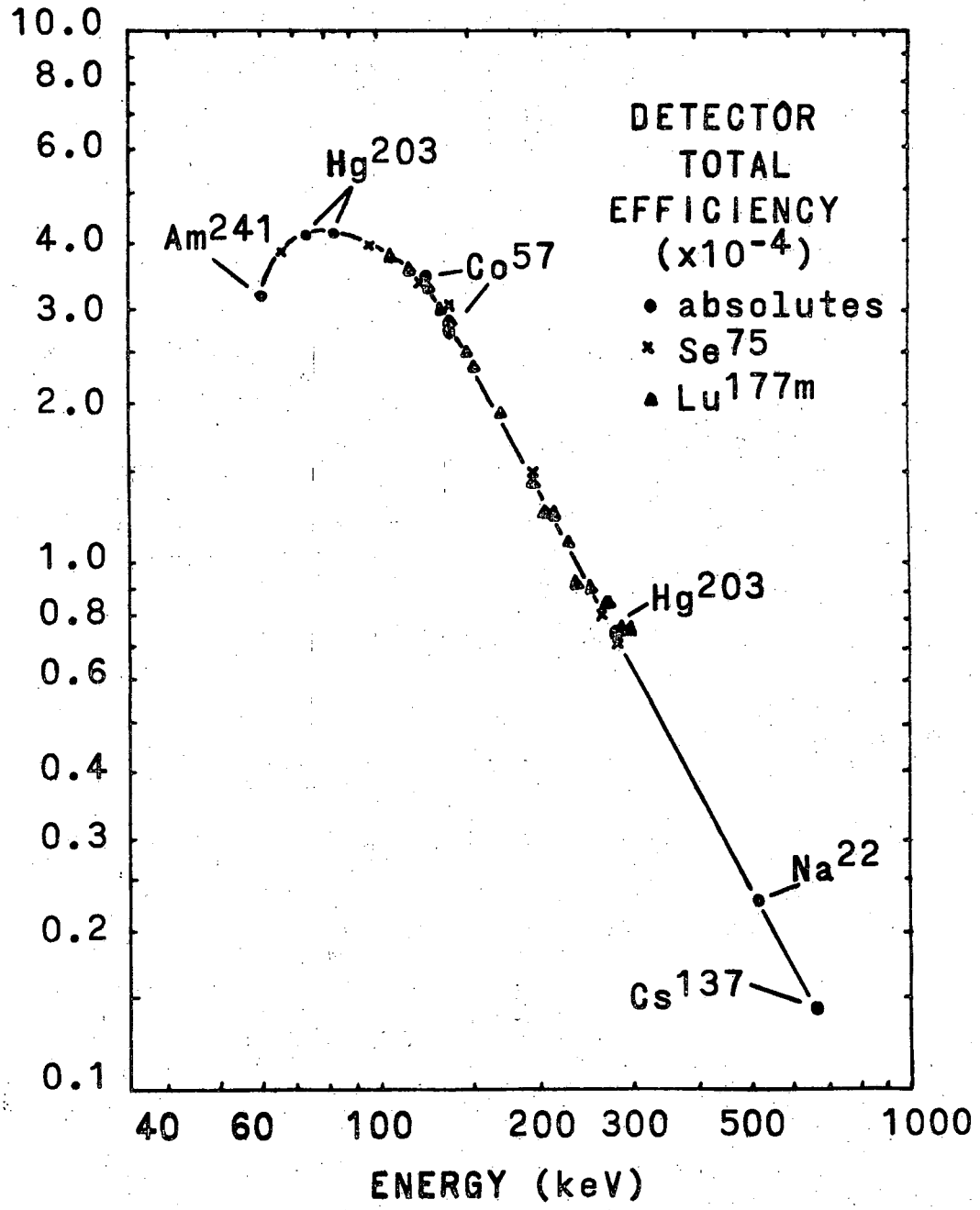

XBL 6811-6218

Fig. 6. Detector total efficency versus energy.

E. Targets

The targets were about the area of the focused pion beam at the table position three feet from the last quadrupole Q2. We selected targets to be as isotopically pure as possible to avoid the problems with lines from several isotopes.

Two criteria restrict the choice of a suitable thickness of material to use as a target. The first criterion is that the target thickness be small so that the self-absorption of the X rays is small. This criterion is more important for large values of the absorption coefficient which occur at the lower energies. We usually constructed the targets to absorb less than 20% of the X rays.

The second criterion is that the target thickness be large enough to stop sufficient pions to produce a significant number of X rays. The detector efficiency is lower at the higher photon energies, hence the higher energies require a thicker target. An occasional consideration which prohibits thick targets is the supply of the desired material. A general compromise led to targets of thicknesses of from one to two gm/cm.

In order to leave the beam on when changing a target we employed a device to change the target by remote control. We also employed a remote control device to change CH_2 degrader material (used to measure the pion range) and thus make frequent checks without affecting the whole cyclotron.

We observed the uniformity of the pion beam over the target area by exposing a photographic film in the pion beam at the target position. We checked that pions stopped uniformly in the depth of the target

by placing several thin target sheets at the target position and observing that the stopped pion rate increased with thickness consistently with the assumption of uniform stopping. By placing in the beam sheets of CH_2 which we called differential range material, we found a position where the number of stopped pions in the target was maximized. Figure 7 shows a differential range curve of the stopped pion scaler reading versus the additional inches of CH_2.

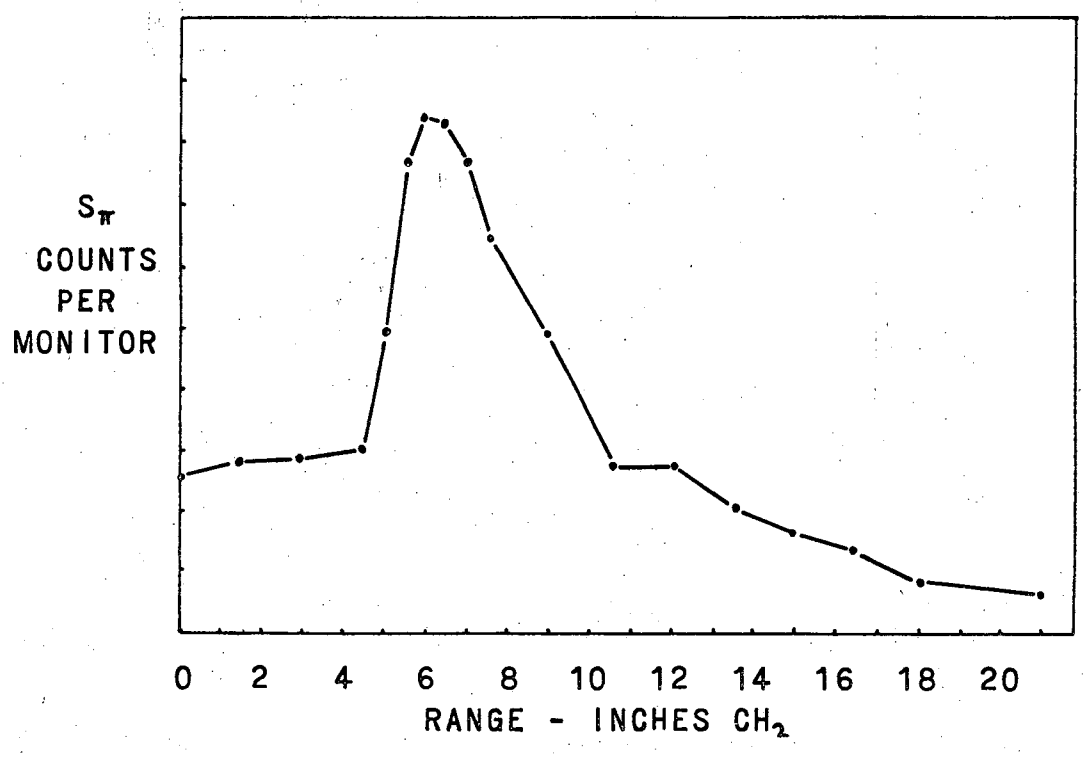

XBL 6812-6253

Fig. 7. Number of π^- stopped in the target (as counted by S_π monitor) as a function of the thickness of CH_2 moderator inserted into the beam (CH_2 block of Fig. 2).

F. Calibration

The characteristics of interest in the X-ray lines observed were the energy, intensity, and width. Radioactive sources have gamma-ray lines with known energy, intensity, and width. When we compared the characteristics of the gamma calibration peaks with the pionic X-ray peaks, we obtained all desired information. Figure 8 and Fig. 9 show calibration spectra. Figure 10 shows a pionic X-ray spectrum.

We used several techniques to find the characteristics of the X-ray peaks in the spectra, but they all involved the same basic procedure. The various methods included 1) an on-line computer program which fitted a Gaussian on a quadratic background to the data,

$$y(x) = a\,x^2 + bx + c + d\,e^{\frac{(x-x_o)^2}{2\sigma^2}}$$

where $y(x)$ is the counts per channel, x is the channel number, a, b, c, d are constants, and σ is the Gaussian width, 2) a computer program which obtained the characteristics by the weighted average of the number of counts above background, and 3) an eye-and-hand method. We checked the various methods against one another and found them consistent.

To obtain the energy calibration we placed several radioactive sources of well known energy[24,25] at the target position. We wanted to avoid any rate effects on the data so the rate was about the same rate as when the X-ray data were being collected. (Channel shifts occur at high rate because the pulses appear on a non-zero baseline.)

The detector efficiency ϵ included the intrinsic efficiency of the germanium detector as well as the effect of the solid angle. As mentioned earlier, we used calibrated radioactive isotopes[24] to carefully measure the detector efficiency. Figure 6 shows the total detector efficiency. Taking the absorption coefficients from the literature,[26,27] we calculated the target transmission T assuming that the pions stopped uniformly. We also directly measured the target transmission using radioactive sources and found agreement with the calculated values.

The statistical error on the number of counts in the peak was usually small. The largest error was the uncertainty in the background subtraction from the peak. Other errors were the uncertainty in the detector efficiency over the large energy interval, and the uncertainty in the target transmission.

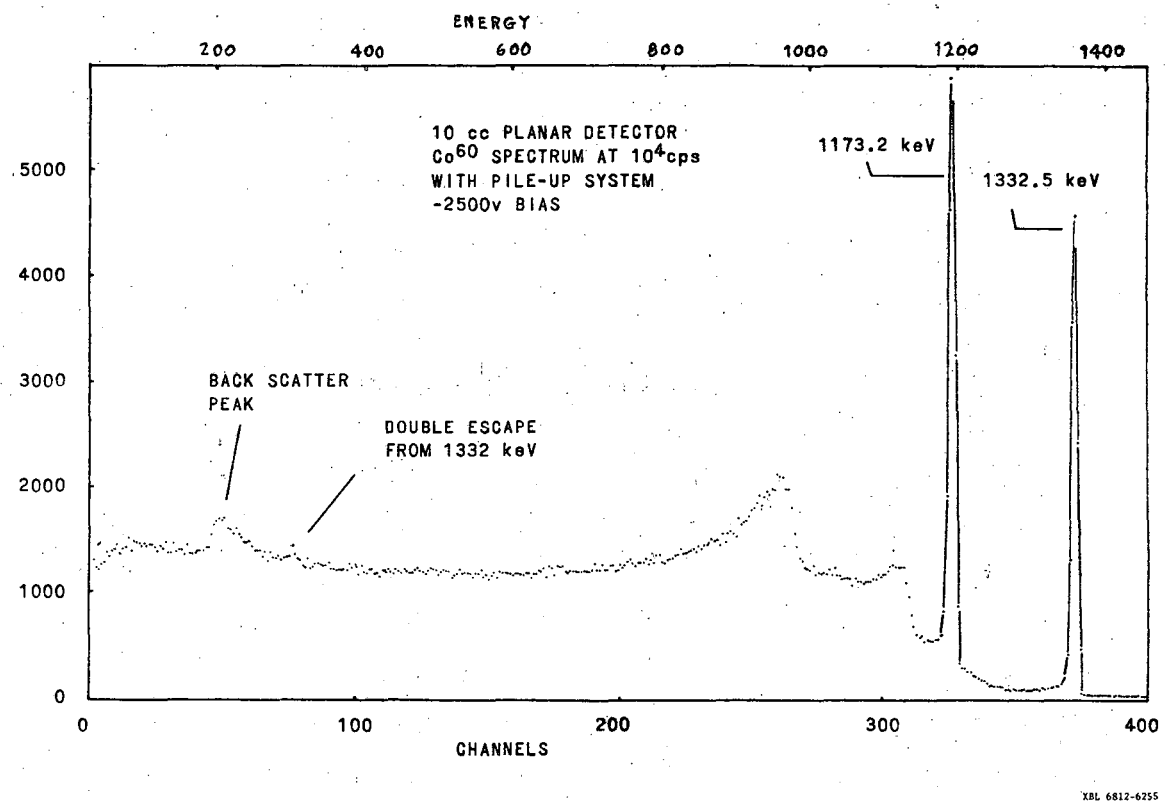

Fig. 8. Calibration source spectrum in counts per channel versus channels. The energy is linearly proportional to the channels and appears along the upper axis. The bumps at 963.4 keV and 1118.1 keV are the Compton peaks of the 1173.2 keV and 1332.5 keV peaks respectively.

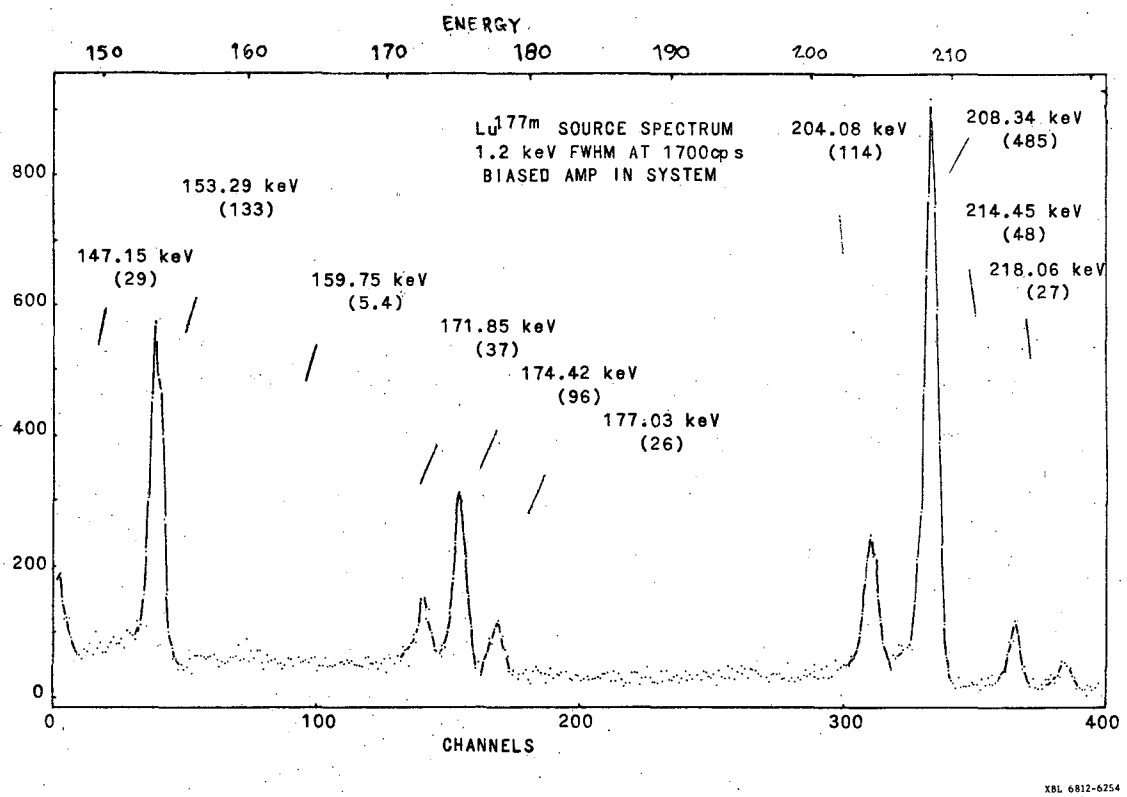

Fig. 9. Calibration source spectrum in counts per channel versus channels. The energy is linearly proportional to the channels and the energy appears along the upper axis.

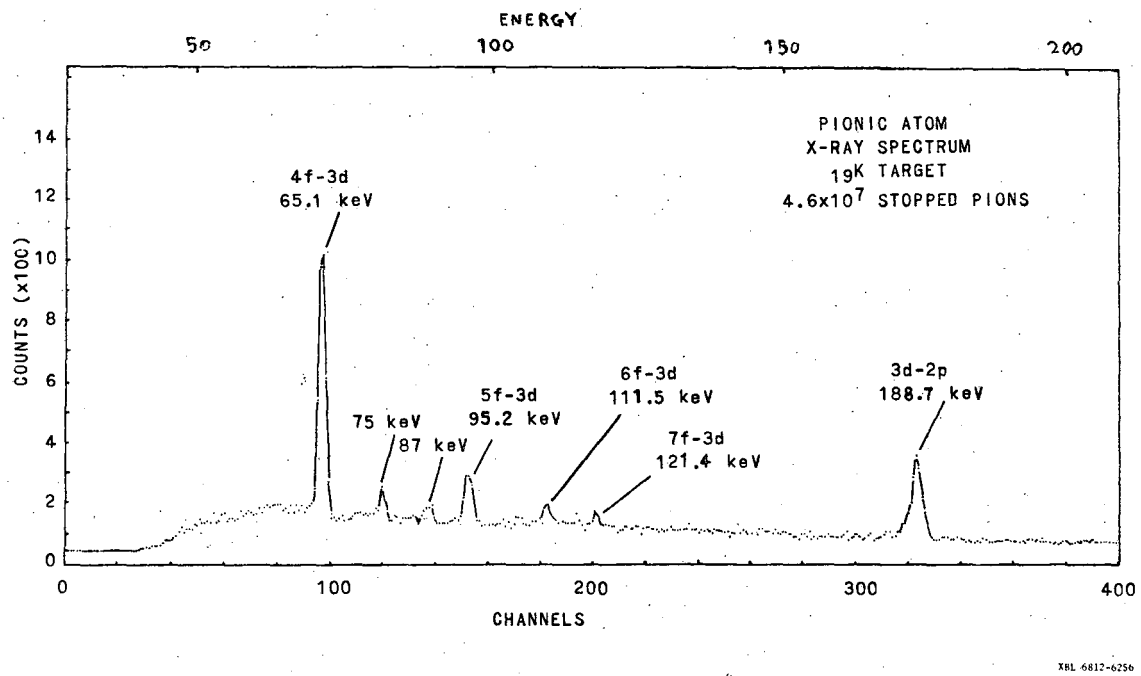

Fig. 10. Pionic X-ray spectrum in counts per channel versus channels. The energy appears along the upper axis.

III. STRONG INTERACTION LINE SHIFTS AND WIDTHS

A. Computation of Pionic X-ray Energies

The measured X-ray energy minus the calculated electromagnetic energy leaves the energy of the strong interaction shift. We calculated the electromagnetic energy by considering all possible non-strong interaction energies which affect the pion nucleus system to a measurable extent.

The main electromagnetic energy is the Klein-Gordon energy E_K. The eigenvalue of the Klein-Gordon equation for level n, ℓ is

$$E_K = \bar{m}c^2 \left[1 + \frac{(\alpha Z)^2}{(n - \ell - \frac{1}{2} + \sqrt{(\ell + \frac{1}{2})^2 - (Z\alpha)^2})^2} \right]^{-1/2} , \quad \text{(III-1)}$$

where $\bar{m}$ is the pion reduced mass, and as shown by Ciafaloni,[28] only the reduced mass $\bar{m} = \frac{m_\pi m_A}{m_\pi + m_A}$ in Eq. (III-1) is necessary in the pion case, where m_A is the mass of the nucleus.

The vacuum polarization is the first correction to the main energy. This correction is large when the pion is close to the nucleus. The closer levels are more tightly bound so the X-ray transition energies are larger than those without the correction. We calculate this energy correction by the formula from Mickelwait and Corben.[29]

The correction for the finite size of the nucleus is the second correction and is large when the pion is near to the nucleus. One calculates the correction by a perturbation method assuming a uniform density for the nucleus given by

$$\rho(r) = \begin{cases} \rho_o & r < R \\ 0 & r > R , \end{cases}$$

where R is the nuclear radius. The closer levels feel the effect more and are less tightly bound than the further levels, so the transition energy of the X rays is lower. We calculate this energy correction by the formula from Pustovalov[30]

$$\Delta E = E_o \left[1 - \frac{1}{(1+\Delta n)^2} \right],$$

where Δn is a function of radius given by Pustovalov and E_o is the energy for the level. Δn is a function of $t=RZ/a$ of the form $\Delta n=P(t)e^{Q(t)}$ where $P(t)$, $Q(t)$ are given by Pustovalov as a result of the perturbation calculation.

The electron screening correction is negligibly small because the pion is far inside the electron shells for the transitions of interest. All other energy corrections are so small as to be negligible for the experiment.

B. Computation of Pionic X-ray Line Widths

The most reasonable assumption was to take the instrumental line shape as Gaussian. The Gaussian instrumental width increased with energy because the detector resolution decreased with energy. The instrumental width varied from about 1.3 keV at low energies (100 keV) to about 4.0 keV at high energies (600 keV).

The natural line shape from the strong interaction was Lorentzian. We obtained the natural line width Γ_n from the measured line width Γ_m (see Appendix for derivation) by the formula for combining a Gaussian and Lorentzian shape.[31]

$$\Gamma_n = \Gamma_m - \frac{\Gamma_i^2}{\Gamma_m} , \qquad \text{(III-2)}$$

where Γ_i is the instrumental width.

C. Experimental Measurements

Table Ia lists the measured energy level shifts and the measured natural line widths of the pionic atom X rays. Figure 11 shows the measured shifts and Fig. 12 shows the measured widths. The label n on each figure is the value of the quantum number n for the level with the given shift or width. The lines go from n+1 to n and the quantum number ℓ is always ℓ=n-1.

Table Ia. Measured energy level shifts and level widths.

Isotope	Shift ΔE_m Berkeley[a]	Shift ΔE_m CERN[b]	Shift ΔE_m W & M[c]	Width Γ_m Berkeley[a]	Width Γ_m CERN[b]	Width Γ_m W & M[c]
n = 1						
$^{4}_{2}He$			-0.07±0.06			0.00±0.09
$^{6}_{3}Li$	-0.6±0.2		-0.35±0.06	0.39±0.36		0.15±0.05
$^{7}_{3}Li$	-0.8±0.2		-0.57±0.06	0.57±0.30		0.19±0.05
$^{9}_{4}Be$	-1.75±0.2	-1.57±0.20	-1.63±0.08	0.85±0.28	1.07±0.30	0.58±0.05
$^{10}_{5}B$	-2.6±0.6	-2.79±0.19	-2.96±0.12	1.4±0.5	1.27±0.25	1.68±0.12
$^{11}_{5}B$	-2.9±0.7	-3.80±0.19	-3.85±0.12	2.3±0.5	1.87±0.25	1.72±0.15
$^{12}_{6}C$	-5.8±0.5	-6.12±0.15	-5.96±0.12	2.6±0.5	2.96±0.25	3.25±0.15
$^{14}_{7}N$	-9.8±1.1	-10.10±0.16		4.1±0.4	4.48±0.30	
$^{16}_{8}O$	-14.7±1.2	-15.73±0.26		9.0±2.0	7.56±0.50	
$^{18}_{8}O$		-20.59±0.26			8.67±0.70	
$^{19}_{9}F$	-25.8±1.1	-25.6±0.6		4.6±2.0[d]	9.4±1.5	
$^{23}_{11}Na$	-49.8±1.4	-52.4±1.0	-51.0±0.5	4.6±3.0[d]	10.3±4.0	6.2±1.2
$^{24}_{12}Mg$	-57.3±1.4					
n = 2						
$^{27}_{13}Al$	0.24±0.08	0.12±0.10			0.36±0.15	
$^{28}_{14}Si$		0.29±0.15				
$^{31}_{15}P$		0.38±0.10			0.43±0.15	
$^{32}_{16}S$	0.7±0.3	0.54±0.10		0.8±0.4	0.79±0.15	
$^{35}_{17}Cl$		0.80±0.15			0.89±0.25	
$^{39}_{19}K$	1.2±0.3	1.44±0.18		1.9±0.6	1.45±0.15	
$^{40}_{20}Ca$	1.76±0.14	1.97±0.18		2.29±0.13	2.0±0.25	
$^{44}_{20}Ca$	1.40±0.10			2.07±0.15		
$^{48}_{22}Ti$		2.27±0.20			2.89±0.25	
$^{51}_{23}V$	2.8±0.4	2.53±0.20			3.66±0.25	
$^{52}_{24}Cr$	2.4±0.5	2.81±0.25			4.46±0.35	
$^{55}_{25}Mn$	2.8±0.8	3.47±0.25			6.38±0.40	
$^{56}_{26}Fe$	4.4±1.0	3.99±0.30		6.0±2.5	8.65±0.60	
$^{59}_{27}Co$	4.1±1.0	4.43±0.35			7.37±0.70	
$^{58}_{28}Ni$		6.04±0.70			12.7±3.0	
$^{63}_{29}Cu$		7.0±2.0			15.9±4.0	
$^{64}_{30}Zn$		8.0±3.0			16.8±6.0	
n = 3						
$^{89}_{39}Y$	0.6±0.3			0.8±0.6		
$^{93}_{41}Nb$	0.6±0.3			0.6±0.4		
$^{103}_{45}Rh$	0.3±0.4			1.2±0.6		
$^{115}_{49}In$	1.8±1.1					
$^{116}_{50}Sn$	2.2±0.6			1.9±1.2		
$^{117}_{50}Sn$	1.7±0.6			2.1±1.2		
$^{118}_{50}Sn$	1.7±0.6			2.5±1.2		
$^{119}_{50}Sn$	1.6±0.6			1.9±1.2		
$^{120}_{50}Sn$	1.8±0.6			2.7±1.2		
$^{122}_{50}Sn$	1.6±0.6			2.0±1.2		
$^{124}_{50}Sn$	1.5±0.6			2.3±1.2		
$^{127}_{53}I$	2.9±1.1					
$^{133}_{55}Cs$	4.0±1.1			4.2±1.8		
$^{139}_{57}La$	5.2±0.9					
$^{140}_{58}Ce$	6.1±2.0			5.8±3.8		
$^{141}_{59}Pr$	7.6±2.0			6.7±2.8		
n = 4						
$^{181}_{73}Ta$	0.0±0.4					
$^{197}_{79}Au$	0.7±0.5					
$^{209}_{83}Bi$	1.8±0.9			1.7±1.0		
$^{232}_{90}Th$	4.5±0.6[d]			6.0±0.9[d]		
$^{238}_{92}U$	6.0±1.1[d]			6.1±1.0[d]		
$^{239}_{94}Pu$	8.2±1.6[d]			9.1±2.5[d]		

[a]Data from Refs. 11, 12, and 13 except Al from Ref. 32.
[b]Data from Refs. 14 and 15.
[c]Data from Ref. 16 except He from Ref. 33 and Na from Ref. 34.
[d]Not used to find optical constants.

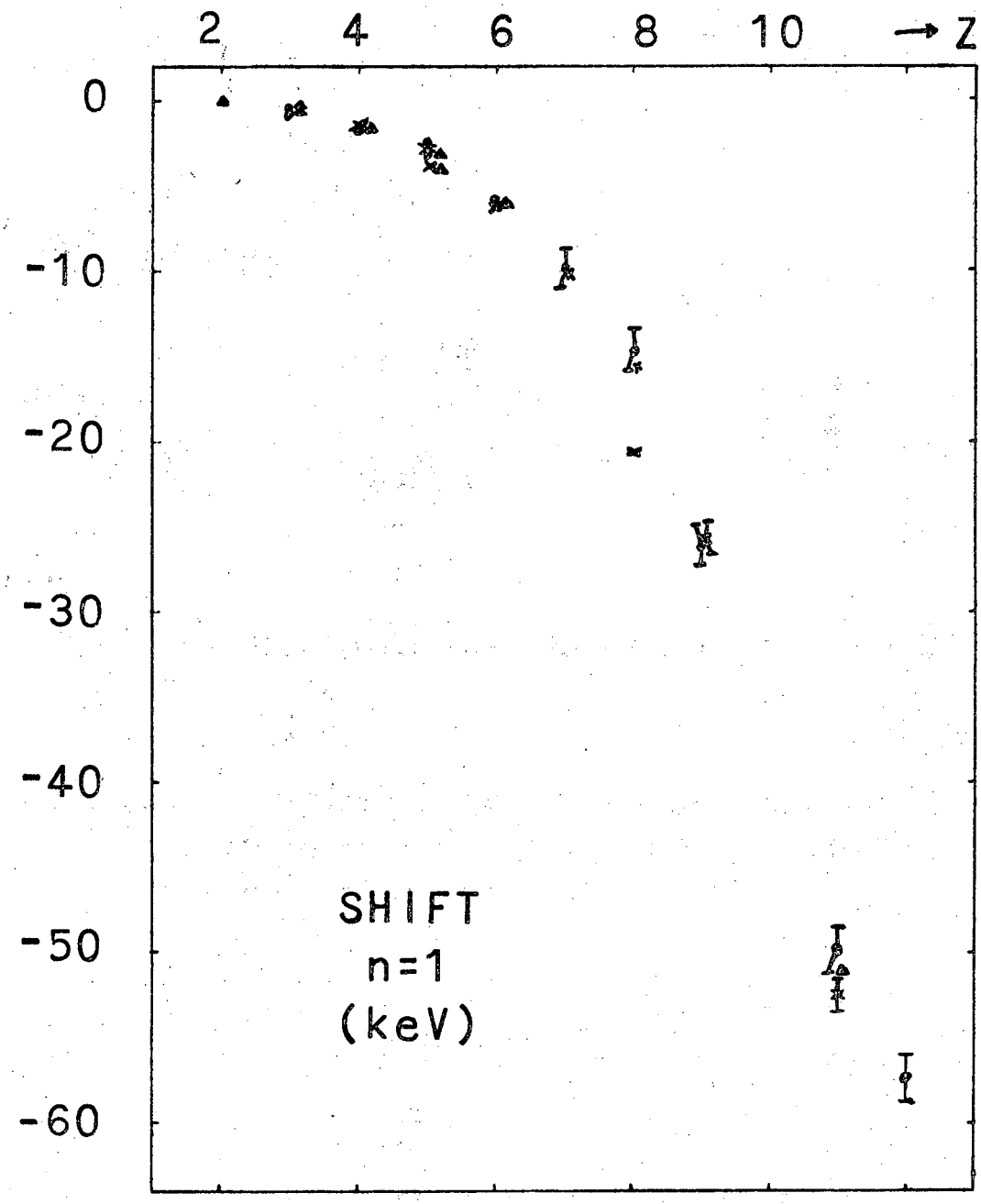

XBL 6812-6245

Fig. 11a. Strong interaction line shift energies. Data plotted as circles are from Berkeley, crosses are from CERN, and triangles are from William and Mary.

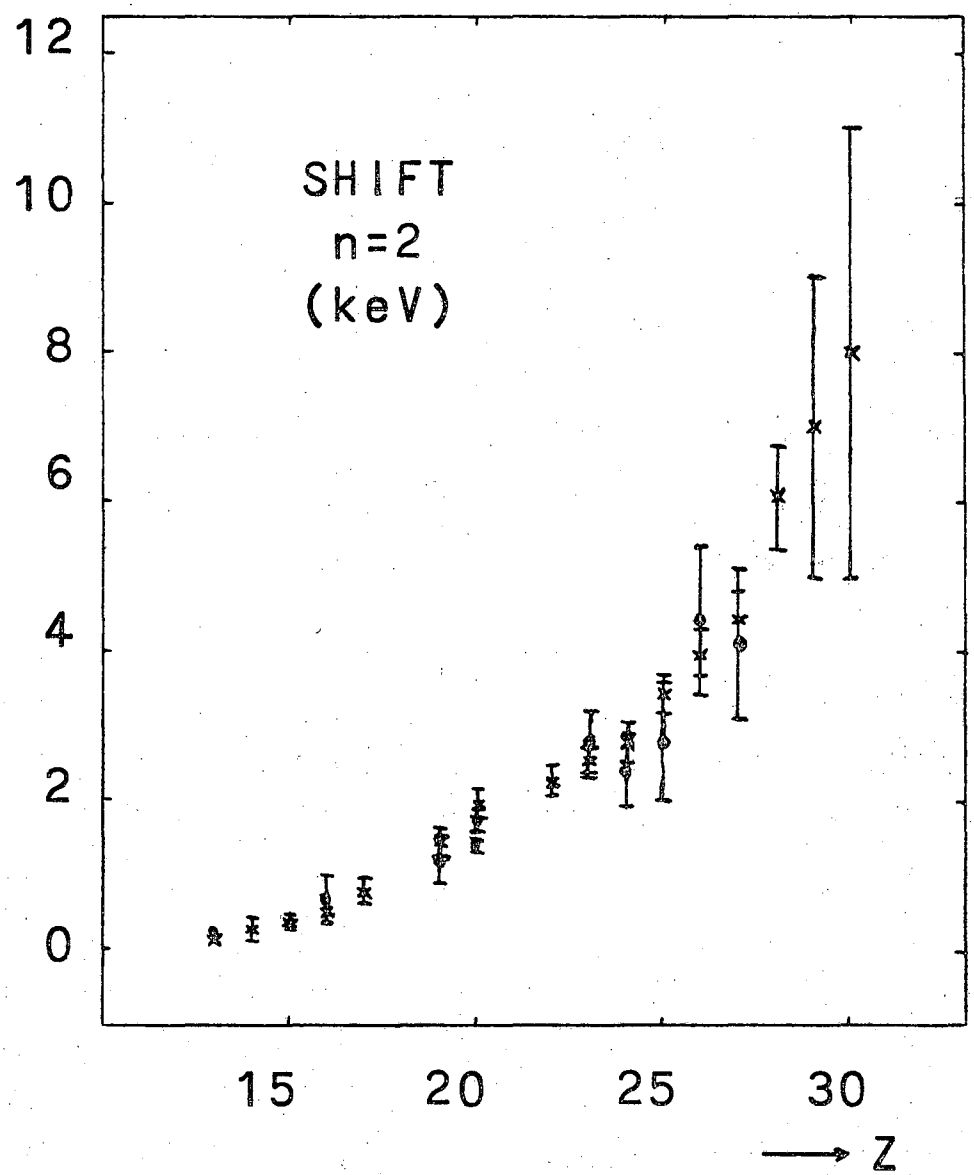

XBL 6812-6246

Fig. 11b. Strong interaction line shift energies. Data plotted as circles are from Berkeley, and crosses are from CERN.

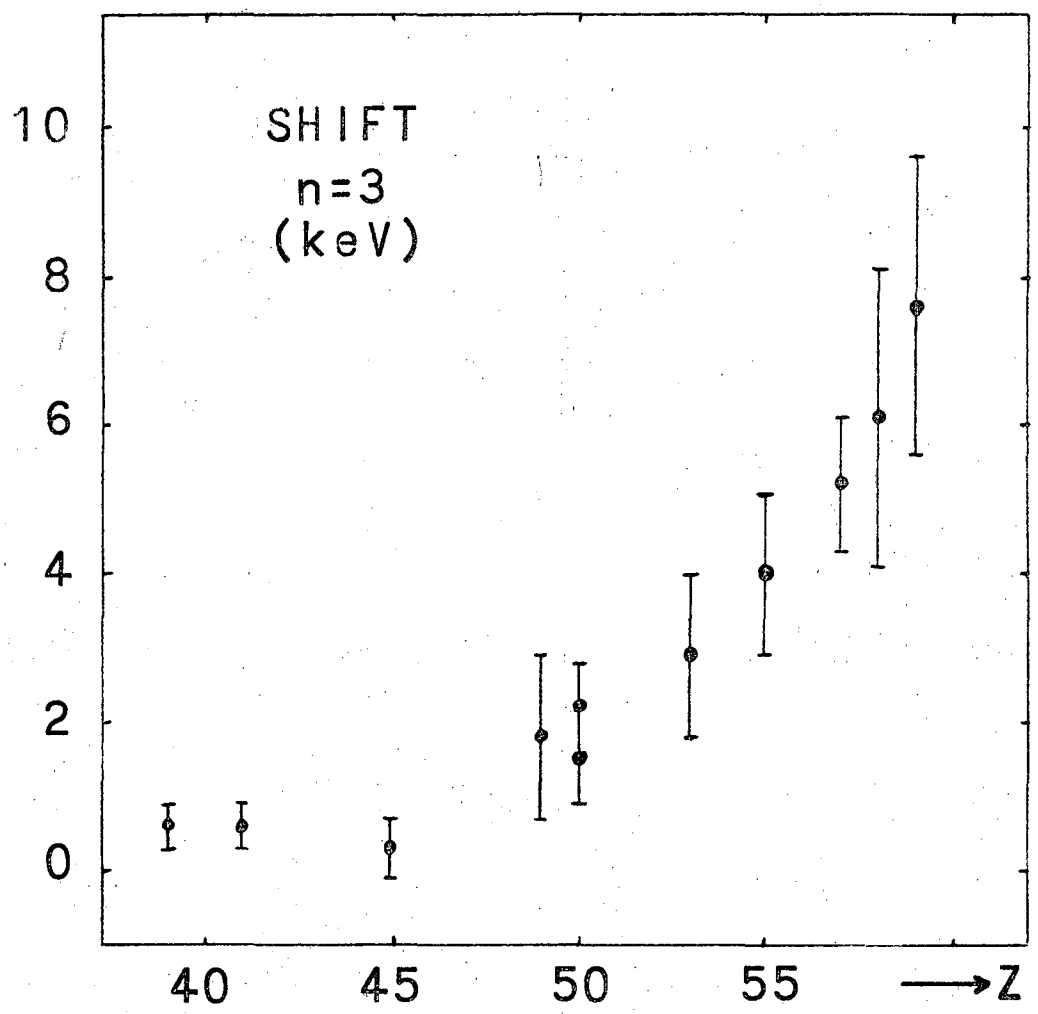

XBL 6812-6247

Fig. 11c. Strong interaction line shift energies. Data plotted as circles are from Berkeley.

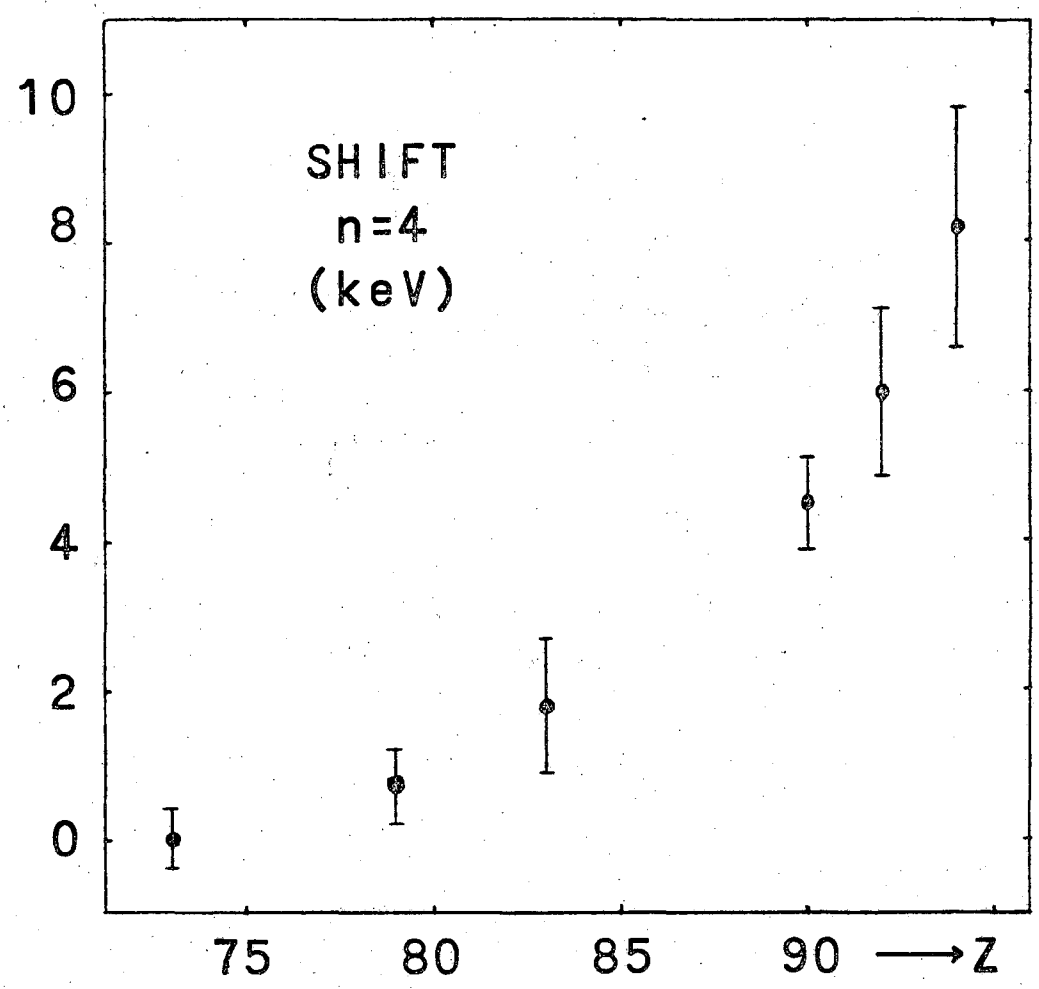

XBL 6812-6257

Fig. 11d. Strong interaction line shift energies. Data plotted as circles are from Berkeley.

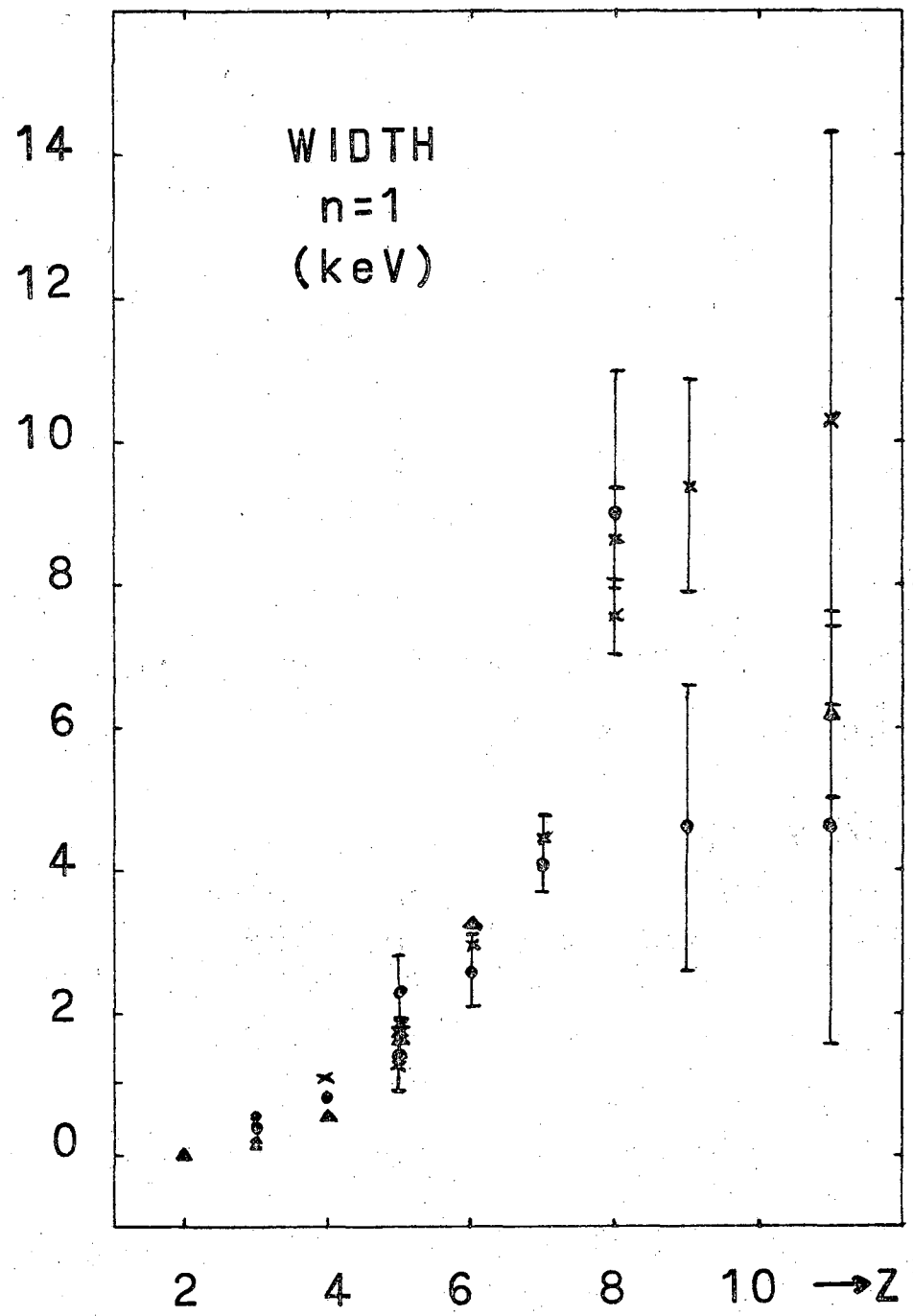

XBL 6812-6241

Fig. 12a. Strong interaction line widths. Data plotted as circles are from Berkeley, crosses are from CERN, and triangles are from William and Mary.

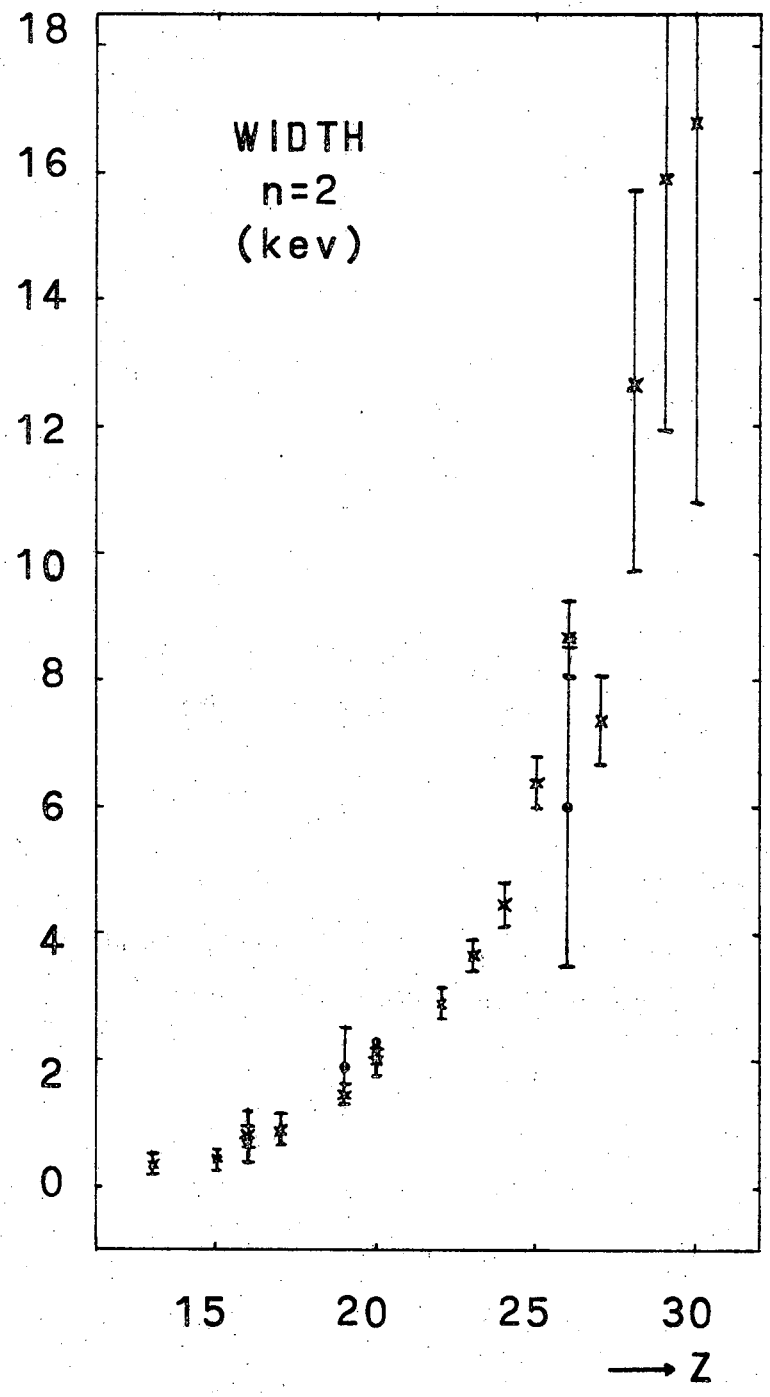

XBL 6812-6242

Fig. 12b. Strong interaction line widths. Data plotted as circles are from Berkeley and crosses are from CERN.

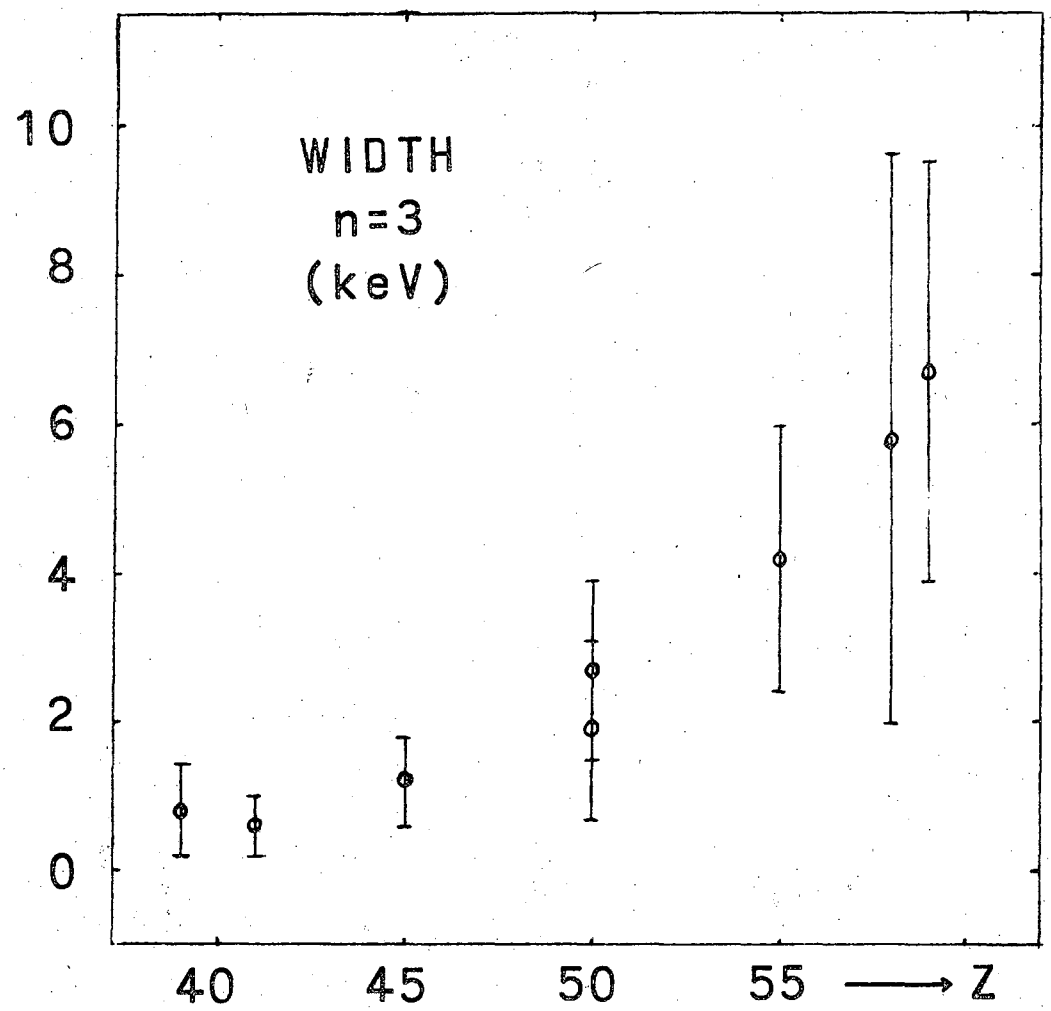

XBL 6812-6243

Fig. 12c. Strong interaction line widths. Data plotted as circles are from Berkeley.

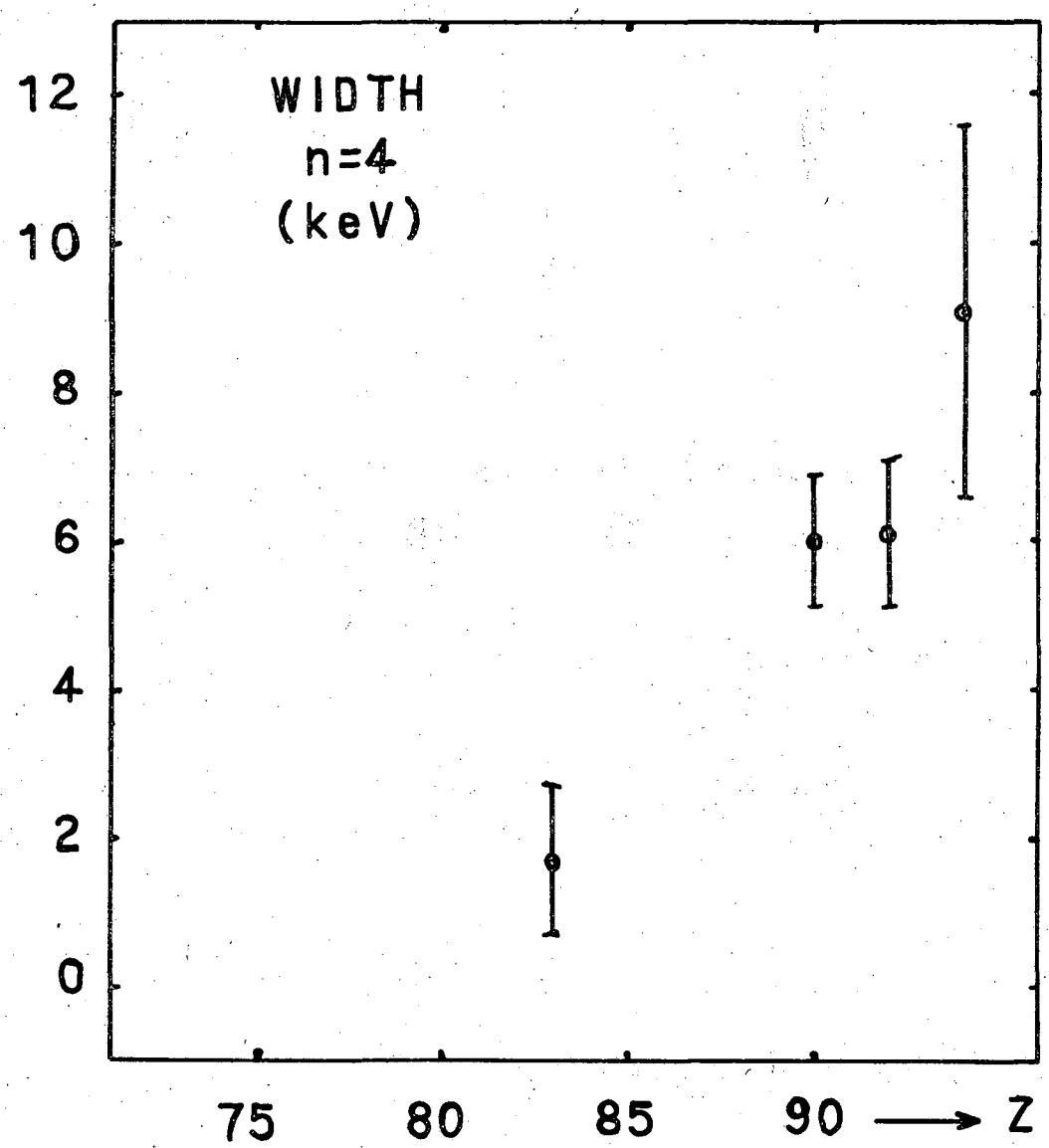

XBL 6812-6244

Fig. 12d. Strong interaction line widths. Data plotted as circles are from Berkeley.

D. Phenomenological Pion-Nuclear Optical Model

1. Introduction

The basic idea of the pion-nuclear optical model is to represent the nucleus by a potential $V(r) = v\,\rho(r)$, where v is a complex operator representing the magnitude of the pion-nuclear interaction and $\rho(r)$ is the spatial density distribution of the potential. When only s-wave and not p-wave πN interaction is considered v will be a number and not an operator. The potential is complex with the imaginary part representing inelastic processes allowed by selection rules and conservation laws. The real part of the potential is connected mainly to the X-ray level shifts and the imaginary part of the potential is connected mainly to the X-ray level widths. We use v, $\rho(r)$ to have a general meaning throughout and v_o, $\rho_o(r)$, v_1, $\rho_1(r)$ to have a specific meaning as explained below. The real and imaginary parts of v_o are u_o, w_o and for v_1 are u_1, w_1.

The simplest form of an optical potential is the square-well potential

$$V(r) = \begin{cases} (u_o - iw_o)\rho_o & r < R \\ 0 & r > R \end{cases}, \qquad \text{(III-3)}$$

where R is the nuclear radius, and ρ_o a normalization constant equal to $3A/4\pi R^3$. We will show that the form of $\rho(r)$ does not greatly affect the interaction by using both the square-well potential and a Saxon-Woods potential

$$V(r) = \frac{v_1\rho_1}{1 + e^{\left(\frac{r-c}{z_1}\right)}}, \qquad \text{(III-4)}$$

where c is called the half-density radius, z_1 the skin thickness para-

meter, ρ_1 a normalization constant, and v_1 a complex operator representing the magnitude of the interaction. One finds ρ_1 from the normalization condition $\int \rho_1(r)dv=A$, where A is the number of nucleons. We add an isotopic spin dependent term to the real parts. The isotopic term is the invariant

$$2\,\frac{\vec{t}\cdot\vec{T}}{A}$$

where $\vec{t}$ is the pion isotopic spin of magnitude 1 and $\vec{T}$ is the nuclear total isotopic spin. By squaring $\vec{t}+\vec{T}$ one finds $\vec{t}\cdot\vec{T}$

$$\vec{t}\cdot\vec{T} = \frac{1}{2}\left[(t+T)(t+T+1)-(t+1)t-(T+1)T\right] = T\ ,$$

we take for T the eigenvalue of $T_3 = \frac{n-Z}{2}$, for n neutrons and Z protons. We also add a term to cover the p-wave nature of the πN interaction and this will be explained in detail later. Using perturbation theory we calculate the pion-nuclear interaction

$$\Delta E + i\Gamma = -\int \psi_\pi^* V(r)\ \psi_\pi\ dv\ , \qquad \text{(III-5)}$$

where ψ_π is the hydrogenic wave function for the pion, Γ is the full width at half maximum of the X-ray line, and ΔE is the shift in X-ray energy.

The equation used for the interaction to calculate the shifts is finally

$$\Delta E(\text{shift}) = \text{Re}(-\int \psi_\pi^* V(r)\ \psi_\pi\ dv) = \qquad \text{(III-6)}$$

$$= \frac{4\pi\hbar^2}{2m}\int\left[(b_o+b_1\,\frac{n-Z}{A})\rho(r)\psi_\pi^2+(c_o+c_1\,\frac{n-Z}{A})\rho(r)|\nabla\psi_\pi|^2\right]dv,$$

where b_o, b_1, c_o, c_1 are constants and the term $\nabla\psi_\pi$ represents the fact the πN interaction has a p-wave character that will be explained further

later. We factor out $\frac{4\pi\hbar^2}{2m}$ for convenience. The equation used for the interaction to calculate the widths is

$$\Gamma(\text{width}) = \text{Im}(-\int \psi_\pi^* V(r)\ \psi_\pi dv) = \tag{III-7}$$

$$= \frac{4\pi\hbar^2}{2m}\left[A_1\int \rho^2(r)|\psi_\pi|^2\ dv + A_2\int \rho^2(r)|\nabla\psi_\pi|^2 dv\right] ,$$

where A_1, A_2 are constants, and $\rho^2(r)$ is the two nucleon density obtained by the square of the one nucleon density. We use $\rho^2(r)$ because the pion must be absorbed by two nucleons. The process $\pi^- p \rightarrow n$ does not conserve energy and momentum. The dominant processes are $\pi^- pp \rightarrow pn$ and $\pi^- pn \rightarrow nn$.

For the purposes of calculating the necessary integrals we assume the radii of the nucleus for the strong interaction and for the electromagnetic interaction are the same because we use radii found by electromagnetic measurements. Table Ib lists the values of the nuclear radii used in the calculations.

Table Ib. Calculated energy level shifts and level widths.

Isotope	Calculated shift ΔE_c	Calculated width Γ_c	Uniform nucleus radius[a]	Saxon-Woods parameters[b] c	z_1
n = 1					
$^{4}_{2}He$	-0.07	0.04	2.07	1.10	1.40
$^{6}_{3}Li$	-0.36	0.07	3.28[c]	1.20	3.08[d]
$^{7}_{3}Li$	-0.50	0.11	3.09	1.43	2.50[f]
$^{9}_{4}Be$	-1.43	0.36	3.25[d]	0.90	3.48[d]
$^{10}_{5}B$	-2.61	0.92	3.16[e]	2.30	2.40[f]
$^{11}_{5}B$	-3.25	1.16	3.12[e]	2.00	2.42[d]
$^{12}_{6}C$	-5.29	2.36	3.11[f]	2.24	2.20[d]
$^{14}_{7}N$	-9.49	4.75	3.16[f]	2.30	2.20
$^{16}_{8}O$	-15.47	7.05	3.42[f]	2.60	1.80
$^{18}_{8}O$	-20.00	7.71	3.58[g]	2.80	2.40
$^{19}_{9}F$	-26.78	10.93	3.68	2.85	2.40
$^{23}_{11}Na$	-54.02	25.37	3.79	3.04	2.40
$^{24}_{12}Mg$	-65.54		3.88	2.93	2.60
n = 2					
$^{27}_{13}Al$	0.16	0.11	3.91[f]	3.21	2.40
$^{28}_{14}Si$	0.26		3.92[f]	3.25	2.40
$^{31}_{15}P$	0.34	0.25	4.08	3.36	2.40
$^{32}_{16}S$	0.52	0.35	4.12[f]	3.26	2.60
$^{35}_{17}Cl$	0.67	0.51	4.25	3.50	2.40
$^{39}_{19}K$	1.19	0.95	4.41	3.63	2.40
$^{40}_{20}Ca$	1.62	1.16	4.54[f]	3.60	2.53[h]
$^{44}_{20}Ca$	1.27	1.44	4.50	3.52	2.57[h]
$^{48}_{22}Ti$	2.00	2.31	4.72	3.89	2.40
$^{51}_{23}V$	2.51	3.37	4.63[f]	3.98	2.20[f]
$^{52}_{24}Cr$	2.96	3.51	4.94	3.99	2.40
$^{55}_{25}Mn$	3.41	4.62	4.97	4.07	2.40
$^{56}_{26}Fe$	4.38	5.41	5.06	4.09	2.40
$^{59}_{27}Co$	5.37	7.61	4.94[f]	4.09	2.50
$^{58}_{28}Ni$	7.41	7.89	5.09[f]	4.14	2.40
$^{63}_{29}Cu$	7.05	10.34	5.17	4.26	2.40
$^{64}_{30}Zn$	8.97	12.14	5.20	4.28	2.40
n = 3					
$^{89}_{39}Y$	0.30	0.30	5.36	4.78	2.40
$^{93}_{41}Nb$	0.45	0.44	5.44	4.85	2.40
$^{103}_{45}Rh$	0.87	0.91	5.63	5.02	2.40
$^{115}_{49}In$	1.50		5.80	5.24	2.30[f]
$^{116}_{50}Sn$	1.78	2.08	5.85	5.22	2.40
$^{117}_{50}Sn$	1.74	2.11	5.87	5.23	2.40
$^{118}_{50}Sn$	1.70	2.13	5.89	5.25	2.40
$^{119}_{50}Sn$	1.66	2.16	5.90	5.26	2.40
$^{120}_{50}Sn$	1.62	2.19	5.92	5.28	2.40
$^{122}_{50}Sn$	1.54	2.24	5.95	5.31	2.40
$^{124}_{50}Sn$	1.45	2.30	5.98	5.34	2.40
$^{127}_{53}I$	2.43		6.03	5.38	2.40
$^{133}_{55}Cs$	3.03	4.51	6.12	5.46	2.40
$^{139}_{57}La$	3.73		6.22	5.54	2.40
$^{140}_{58}Ce$	4.34	6.63	6.23	5.55	2.40
$^{141}_{59}Pr$	5.03	7.39	6.25	5.57	2.40
n = 4					
$^{181}_{73}Ta$	0.23		7.10[f]	6.45	2.80[f]
$^{197}_{79}Au$	0.43		6.87[f]	6.38	2.32[f]
$^{209}_{83}Bi$	0.67	0.92	7.13[f]	6.47	2.70[f]

[a] $R = r_0 A^{1/3}$, where $r_0 = 1.3$ for $Z < 39$ and $r_0 = 1.2$ for $Z > 39$, except where reference noted.

[b] From Ref. 42. [c] Reference 35. [d] Reference 36. [e] Reference 37. [f] Reference 38.

[g] Reference 39. [h] Reference 40.

2. Experimentally determined optical constants

We determined the optical model constants b_o, b_1, c_o, c_1 by a least squares fit[41] to the experimental measurements. Table Ib lists the calcualted energy level shifts and calculated level widths from the fitting procedure.

With some isotopes we observed an energy-level splitting caused by the magnetic dipole and electric quadrupole moments of the nucleus. These included ^{51}V, ^{52}Cr, ^{55}Mn, ^{115}In, ^{127}I, ^{139}La, ^{181}Ta, ^{197}Au, ^{232}Th, ^{238}U, ^{239}Pu. Since these splittings were not well resolved by the detectors, they confused the measurements of level widths. We restricted the analysis to the level broadenings of those isotopes with splittings that were calculated to be less than 0.3 keV, except bismuth, which had a splitting of 0.6 keV.

a. Shifts

Assuming a square-well potential for the nucleus, the experimentally determined optical model constants from the least squares fit to the energy level shifts were (in units of $\lambda\!\!\!^{-} = \frac{\hbar}{m_\pi c} = 1.41$ fm)

$$b_o = -0.01915 \pm 0.00014 \quad (\lambda\!\!\!^{-}) \qquad \text{(III-8)}$$
$$b_1 = -0.0261 \pm 0.0027 \quad (\lambda\!\!\!^{-})$$
$$c_o = +0.1388 \pm 0.0039 \quad (\lambda\!\!\!^{-3})$$
$$c_1 = -0.2626 \pm 0.0445 \quad (\lambda\!\!\!^{-3})$$

Assuming a Saxon-Woods potential for the nucleus, the experimentally determined constants were

$$b_o = -0.01902 \pm 0.00014 \quad (\lambda) \qquad \text{(III-9)}$$
$$b_1 = -0.02749 \pm 0.0027 \quad (\lambda)$$

$$c_o = +0.1289 \pm 0.0038 \qquad (\lambda\!\!\!^{-3})$$

$$c_1 = -0.2162 \pm 0.0444 \qquad (\lambda\!\!\!^{-3}) .$$

No dependence on nuclear model was apparent.

To test for a spin dependent optical model term proportional to $\vec{\ell}\cdot\vec{J}$ where $\vec{\ell}$ is the pion angular momentum and $\vec{J}$ the nuclear spin, we made another least squares fit to only the measured energy level shifts for nuclei having zero spin or for pion levels of zero angular momentum. The result assuming a uniform potential for the nucleus was

$$b_o = -0.01942 \pm 0.00019 \quad (\lambda\!\!\!^{-}) \qquad \text{(III-10)}$$

$$b_1 = -0.0276 \pm 0.0031 \quad (\lambda\!\!\!^{-})$$

$$c_o = +0.1416 \pm 0.0045 \quad (\lambda\!\!\!^{-3})$$

$$c_1 = -0.2811 \pm 0.058 \quad (\lambda\!\!\!^{-3}) .$$

No dependence on spin was apparent. In conclusion the values are all about the same and we may assume as our empirically determined b_o, b_1, c_o, c_1, Eq. (III-8).

b. <u>Widths</u>

The experimentally determined optical model constants from the least squares fit to the level widths assuming a uniform nuclear model were (in units of $\lambda\!\!\!^{-}$)

$$A_1 = 0.0310 \pm 0.0007 \qquad (\lambda\!\!\!^{-4}) \qquad \text{(III-11)}$$

$$A_2 = 0.1711 \pm 0.0062 \qquad (\lambda\!\!\!^{-6}).$$

3. Predictions for optical model constants

Assuming the πN (pion-nucleon) interactions in the nucleus are the same as for free nucleons, the Ericsons[9] developed a detailed multiple scattering theory for low energy pions. I will develop a simple example to show the line of argument but refer the reader to their paper for full mathematical details.

At low energies an s-wave interaction alone does not explain the measured angular distribution of pion-nucleon scattering. The Ericsons allow for an s- and p-wave part to the interaction.[9] The influence of d and f wave πN scattering on the energy level shifts is negligible[42] with the present precision of measurement. The Ericsons assume the πN scattering amplitude with s- and p-waves is

$$f_i(\theta) = [b_o + c_o \vec{k}'\cdot\vec{k}]\delta(\vec{r}-\vec{r}_i), \qquad \text{(III-12)}$$

where i refers to the ith nucleon, b_o and c_o are constants for the s- and p-wave amplitudes, and $\vec{k}$, $\vec{k}'$ are the initial and final pion momenta. This assumption is not certain. The assumption of constants and this momentum dependence may be incorrect for bound pions interacting with the nucleus. One obtains the scattering amplitude for the nucleus by summing over all i nucleons. This gives

$$f = [b_o + c_o \vec{k}'\cdot\vec{k}]\hat{\rho}(\vec{r})$$

where

$$\hat{\rho}(\vec{r}) = \sum_i \delta(\vec{r}-\vec{r}_i)$$

is the density of nucleons in the nucleus.

From the scattering amplitude one derives the potential using the

Born approximation

$$f(\theta) = \frac{-2m}{4\pi\hbar^2}\int e^{-i\vec{k}'\cdot\vec{r}}\, V(\vec{r})\, e^{i\vec{k}\cdot\vec{r}}\, d\vec{r} \ , \qquad \text{(III-13)}$$

where m is the pion reduced mass.

One inverts the equation to solve for the potential

$$V(\vec{r}) = \frac{-4\pi\hbar^2}{2m}\int f(\theta)\, e^{-i(\vec{k}-\vec{k}')\cdot\vec{r}}\, d(\vec{k}-\vec{k}') \ . \qquad \text{(III-14)}$$

One puts the scattering amplitude into the equation and solves for the potential using the fact that

$$\vec{k} = -i(\nabla e^{i\vec{k}\cdot\vec{r}})e^{-i\vec{k}\cdot\vec{r}} \ .$$

The potential operator becomes

$$V(\vec{r}) = \frac{-4\pi\hbar^2}{2m}\left[b_o\rho(\vec{r}) - c_o\nabla\cdot\rho(\vec{r})\nabla\right], \qquad \text{(III-15)}$$

where $V(\vec{r})$ is an operator which appears between the initial and final wave functions, $\rho(\vec{r})$ is the average nucleon density in the nucleus (either Saxon-Woods or uniform), and the gradient ∇ operates on the wave function. The next step is to use the vector identity

$$\psi^*\nabla\cdot\rho(r)\nabla\psi = \nabla\cdot(\psi^*\rho(r)\nabla\psi) - \nabla\psi^*\cdot\rho(r)\nabla\psi \ , \qquad \text{(III-16)}$$

and to realize finally that the first term on the right of Eq. (III-16) will contribute nothing in the integral,

$$\int_{(v)} \nabla\cdot(\psi^*\rho(r)\nabla\psi)dv =$$

$$= \int_{(s)} \psi^*\rho(r)\nabla\psi\cdot\hat{n}da = 0 \ .$$

This potential is the basic form but one adds isotopic spin dependent terms. As mentioned earlier, the isotopic term is the

invariant $2\,\frac{\vec{t}\cdot\vec{T}}{A}$, where $\vec{t}$ is the pion isotopic spin, $\vec{T}$ is the nuclear isotopic spin and $\vec{t}\cdot\vec{T}$ is equal to the eigenvalue $T_3 = \frac{n-Z}{2}$. The Ericsons also calculated a spin dependent term that they expected to be small[9] (proportional to $\vec{\ell}\cdot\vec{J}$, where $\vec{\ell}$ is the pion angular momentum and $\vec{J}$ the nuclear spin). We showed earlier that it is small.

Using similar considerations as for the shifts we now consider the widths. As explained earlier, the pion cannot be absorbed by one nucleon and conserve momentum so to explain absorption one needs $\pi NN \rightarrow NN$. The scattering amplitude for this interaction is of the form

$$f_{ij}(\theta) = (B_o + C_o\,\vec{k}\cdot\vec{k}')\delta(\vec{r}_i-\vec{r}_j)\;\delta(\vec{r} - \tfrac{1}{2}(\vec{r}_i+\vec{r}_j)) \;, \qquad \text{(III-17)}$$

where i, j refer to the two nucleons that must be close together and B_o, C_o are complex constants. Using this amplitude one derives a potoential with $\rho^2(\vec{r})$, which is intuitively reasonable because the density of pairs of nucleons is proportional to $\rho^2(\vec{r})$. The imaginary part of this amplitude comes from $\pi NN \rightarrow NN$ and explain the widths. The real part of this potential comes from $\pi NN \rightarrow \pi NN$ and is a negligible contribution to the level shifts.

In order to summarize the recent discussion we used as a formula to explain the strong-interaction level shifts

$$\Delta E = \frac{-4\pi\hbar^2}{2m}\int\left[(b_o + b_1\,\frac{n-Z}{A})\rho(r)|\psi_\pi|^2 + (c_o + c_1\,\frac{n-Z}{A})\rho(r)|\nabla\psi_\pi|^2\right]dv \;, \qquad \text{(III-18)}$$

which is the same as Eq. (III-6) where b_o, b_1, c_o, c_1 are constants given by the Ericsons as combinations of πN scattering lengths and volumes and m is the reduced mass. We used as a formula to explain the level widths

$$\Gamma = \frac{4\pi\hbar^2}{2m}\left[A_1 \int \rho^2(\vec{r})|\psi_\pi|^2 dv + A_2 \int \rho^2(\vec{r})|\nabla\psi_\pi|^2 dv \right] , \qquad \text{(III-19)}$$

which is the same as Eq. (III-7) where Γ is the full width at half maximum, A_1, A_2 have values predicted by M. Ericson[43] and $\rho^2(\vec{r})$ is the two nucleon density obtained by the square of the one nucleon density.

According to the Ericsons the πN scattering lengths a_{2t} and volumes $a_{2t,2j}$ should combine to give the optical model constants[9] as follows

$$\begin{aligned} b_o &= 1/3\ (a_1 + 2a_3) \qquad \text{(III-20)} \\ b_1 &= 1/3\ (a_3 - a_1) \\ c_o &= 1/3\ (4a_{33} + 2a_{31} + 2a_{13} + a_{11}) \\ c_1 &= 1/3\ (2a_{33} + a_{31} - 2a_{13} - a_{11}) , \end{aligned}$$

where t is the isospin and j the spin of the πN system.

Recent values of the πN lengths and volumes (given in units of $\lambda\!\!\!^{-} = \hbar/m_\pi c$) are

$$\begin{aligned} a_1 &= 0.1957 \pm 0.0111^{44} \quad (\lambda\!\!\!^{-}) \qquad \text{(III-21)} \\ a_3 &= -0.0700 \pm 0.0054^{44} \quad (\lambda\!\!\!^{-}) \\ a_{11} &= -0.101 \pm 0.007^{45} \quad (\lambda\!\!\!^{-3}) \\ a_{13} &= -0.029 \pm 0.005^{45} \quad (\lambda\!\!\!^{-3}) \\ a_{31} &= -0.038 \pm 0.005^{45} \quad (\lambda\!\!\!^{-3}) \\ a_{33} &= 0.215 \pm 0.005^{45} \quad (\lambda\!\!\!^{-3}) . \end{aligned}$$

One has for the optical model constants[12] (in $\lambda\!\!\!^{-}$ units)

$$\begin{aligned} b_o &= -0.028 \pm 0.006 \quad (\lambda\!\!\!^{-}) \qquad \text{(III-22)} \\ b_1 &= -0.10 \pm 0.01 \quad (\lambda\!\!\!^{-}) \\ c_o &= 0.19 \pm 0.02 \quad (\lambda\!\!\!^{-3}) \\ c_1 &= 0.16 \pm 0.01 \quad (\lambda\!\!\!^{-3}) . \end{aligned}$$

M. Ericson obtained a prediction of the level widths[43] from π production in NN collisions ($NN \rightarrow NN\pi$) by detailed balance and charge independence. M. Ericson predicted A_1, A_2 to be (in $\lambda\!\!\!^{-}$ units)

$$A_1 = 0.0471 \pm 0.0053 \quad (\lambda\!\!\!^{-4}) \qquad \text{(III-23)}$$

$$A_2 = 0.342 \pm 0.081 \quad (\lambda\!\!\!^{-6})$$

A recent low energy cross section measurement[46] gives a new value for A_1 as discussed by Harris[47]

$$A_1 = 0.0348 \pm 0.0043 \quad (\lambda\!\!\!^{-4}) \quad . \qquad \text{(III-24)}$$

E. Comparison of Theory and Experiment

We tabulate below the differences between the predictions (III-22), (III-23), (III-24) and the experimentally determined constants (III-8) and (III-11).

	Theory	Experiment	Difference (sum of errors from both the experimental and claimed theoretical numbers)	
b_o	-0.028	-0.019	-0.009 ± 0.006	(λ)
b_1	-0.10	-0.026	-0.084 ± 0.013	(λ)
c_o	+0.19	+0.139	+0.051 ± 0.024	(λ^3)
c_1	+0.16	-0.263	+0.423 ± 0.055	(λ^3)
				(III-25)
A_1	0.0348	0.0310	+0.0038 ± 0.0050	(λ^4)
A_2	0.342	0.171	+0.171 ± 0.0872	(λ^6)
				(III-26)

The non-isotopic terms b_o, c_o agree between theory and experiment. They also agree with the results of the earlier measurements[13] (-0.0197, 0.131). The isotopic spin terms b_1, c_1 disagree between theory and experiment. The experimental are of the same sign as the earlier measurements, though now more precise. The main difference between theory and experiment is in the sign of the isotopic term c_1. Theory predicts the opposite sign to that experimentally determined. The width constants A_1, A_2 agree satisfactorily between theory and experiment considering the assumptions in the theory.

We have three items to point out concerning the differences between theory and experiment. First, the published values of the

πN scattering lengths and volumes are still uncertain and hence the predicted constants also are uncertain. Second, as pointed out earlier, the assumption of the specific dependence of the scattering amplitude on the s- and p-wave scattering amplitudes may be wrong. Third, we use a first-order perturbation calculation to obtain the experimental constants. Seki and Cromer[48] show that the meson probability inside the nucleus has only about half the value given by a first-order perturbation calculation and hence the values we derive from the experimental data for b_o, b_1, c_o, c_1 using perturbation theory would be different from what would be obtained with the wave functions modified to give the different probabilities.

Seki and Cromer question the need for an isotopic spin term, but contrary to Seki and Cromer,[48] isotopic spin terms appear necessary to fit the data. Their conclusions are based on calculations with only the earlier pionic X-ray measurements.[11] As shown previously the need for a spin dependent term is not evident because the constants have the same values whether one uses only the data with no spin or angular momentum for the calculations or all of the data for the calculations. On the whole the agreement appears not satisfactory, but the assumptions put into the theory are considerable.

IV. X-RAY YIELDS OF THE ELEMENTS

A. Method

We define the yield as the number of pionic X rays of a particular pionic transition produced per stopped pion. The yield is a number between zero and one. The number of X rays appearing in a peak of the spectrum is not the true number of X rays of a particular transition because of target absorption of the X rays and the less than 100% detector efficiency, ϵ. The relative yields were more precise because of cancellations of some uncertainties as will be seen later. Many of the measurements were under conditions where the primary interest was in obtaining the X-ray shifts and widths. Thus low energy measured yields were less accurate because of possible pulse losses and pile-up effects.

When no target was in the beam the stopped pion scaler registered counts. These background counts were from pions acting as stopped pions caused by scattering out of the beam before the anti-counter or by stopping in material of the counters. We corrected the number of stopped pions S_π for this target out background. The number of X rays produced divided by the number of stopped pions is the yield. The measured yield is thus

$$Y = \frac{N}{S_\pi \epsilon T} \quad , \qquad \text{(IV-1)}$$

where N is the number of $n_1 \rightarrow n_2$ X rays appearing in the peak of the spectrum, and T is the transmission of X rays out of the target. Table 2 lists the measured transition yields.

We repeated some of the measurements in two independent experi-

mental situations and Fig.13 shows both data as well as data from William and Mary[49] and CERN.[50] As can be seen in the figures, the yields agree where two measurements of the yield of an element were made.

The radiative yield Y_r from level $n_1\ell_1$ to level $n_2\ell_2$ for a given atomic number Z is

$$Y_r = P(n_1\ell_1)\,\frac{R_r}{R_{rt}+R_a+R_n} \qquad \text{(IV-2)}$$

where $P(n_1\ell_1)$ is the probability of a captured pion reaching the level $n_1\ell_1$, R_r is the rate of the radiative process from level $n_1\ell_1$ to level n_2L_2, R_{rt} is the rate of the total radiative processes from level $n_1\ell_1$, R_a is the rate of Auger electron emission for the pion in the level $n_1\ell_1$, and R_n is the rate of nuclear capture from level $n_1\ell_1$. Other processes such as pion decay and collision de-excitation of the atom are small rates in comparison to the three processes considered (with the possible exception of the case of hydrogen which was not measured).

The radiative rates are the electric dipole rates since the higher order multipoles are negligible in comparison. The radiative rates are taken from hydrogen[51] and scaled by $\frac{m_\pi}{m_e} Z^4$ to give

$$R_r = R_r(Z=1,e^-)\left(\frac{m_\pi}{m_e}\right)Z^4 \quad , \qquad \text{(IV-3)}$$

where $R_r(Z=1,e^-)$ is the rate of the radiative process from state $n_1\ell_1$ to state $n_2\ell_2$ for hydrogen. For circular orbits where $n=\ell+1$, one has $R_{rt}=R_r$.

Table II. Measured yields of pionic atoms.
(The yields listed on a second line is the recent measurement.)

Element	2p - 1s	3d - 2p	4f - 3d	5g - 4f	6h - 5g	7i - 6h	8j - 7i
$_{3}Li$	0.26±0.05[a]						
$_{4}B$		0.34±0.04[a]					
$_{6}C$	0.082±0.006	0.44±0.05[a]					
$_{7}N$	0.068±0.008[b]						
$^{16}_{8}O$	0.049±0.007[b]						
$^{18}_{8}O$	0.056±0.008[b]						
$_{9}F$	0.061±0.010[b]						
$_{11}Na$	0.033±0.007[b]						
$_{12}Mg$		0.54±0.05[a]					
$_{14}Si$		0.396±0.045					
$_{15}P$		0.342±0.038					
$_{16}S$		0.346±0.034 0.414±0.062					
$_{19}K$		0.384±0.034 0.298±0.032	0.268±0.061 0.360±0.050				
$_{20}Ca$		0.261±0.023 0.223±0.024	0.273±0.052 0.290±0.030				
$_{22}Ti$		0.203±0.022 0.188±0.028	0.299±0.062 0.288±0.050				
$_{24}Cr$		0.143±0.014	0.232±0.026				
$_{25}Mn$			0.183±0.029				
$_{26}Fe$		0.049±0.005	0.253±0.028 0.219±0.028				
$_{27}Co$		0.052±0.007					
$_{28}Ni$			0.271±0.030				
$_{29}Cu$			0.355±0.035 0.290±0.040	0.215±0.026			
$_{30}Zn$			0.482±0.033 0.358±0.053	0.280±0.062			
$_{31}Ga$			0.463±0.051	0.205±0.023			
$_{32}Ge$			0.576±0.091 0.478±0.054	0.405±0.092 0.302±0.037			
$_{33}As$				0.330±0.039			
$_{34}Se$			0.483±0.054 0.454±0.049	0.305±0.035			
$_{38}Sr$			0.438±0.049	0.382±0.043			
$_{40}Zr$			0.448±0.041 0.403±0.050	0.433±0.074 0.364±0.054	0.410±0.065		
$_{41}Nb$			0.358±0.082	0.304±0.040			
$_{42}Mo$			0.347±0.034	0.291±0.028			
$_{45}Rh$			0.360±0.040	0.413±0.046	0.416±0.047		
$_{46}Pd$				0.362±0.036	0.342±0.038		
$_{47}Ag$			0.293±0.028	0.386±0.032	0.380±0.042		
$_{48}Cd$			0.281±0.031	0.470±0.058 0.340±0.051	0.480±0.051 0.414±0.062		
$_{49}In$			0.376±0.042	0.448±0.045	0.540±0.060		
$_{50}Sn$			0.297±0.033 0.346±0.051	0.634±0.071 0.483±0.053	0.547±0.061 0.418±0.050		
$_{51}Sb$			0.298±0.029	0.474±0.046	0.518±0.058		
$_{52}Te$			0.201±0.022	0.418±0.047	0.385±0.043		
$_{53}I$			0.169±0.99	0.450±0.043	0.469±0.053		
$_{66}Dy$				0.442±0.068	0.447±0.059	0.401±0.061	
$_{67}Ho$				0.391±0.066	0.559±0.061	0.446±0.053	
$_{73}Ta$				0.351±0.035	0.398±0.034		
$_{74}W$				0.394±0.038	0.456±0.044	0.387±0.044	0.224±0.036
$_{76}Os$				0.349±0.039	0.514±0.057	0.334±0.037	0.170±0.019
$_{77}Ir$				0.397±0.039	0.517±0.082	0.353±0.056	
$_{78}Pt$				0.502±0.084	0.424±0.041	0.380±0.042	0.239±0.027
$_{79}Au$				0.361±0.035 0.364±0.054	0.421±0.041 0.483±0.057	0.411±0.041 0.492±0.059	0.217±0.021
$_{81}Tl$				0.381±0.037	0.581±0.056	0.545±0.061	0.286±0.032
$_{82}Pb$				0.392±0.034	0.465±0.040	0.462±0.040	0.328±0.029
$_{83}Bi$				0.402±0.048	0.548±0.056	0.451±0.049	0.279±0.031
$_{90}Th$				0.177±0.021	0.342±0.036	0.295±0.036	0.223±0.028
$_{92}U$				0.184±0.022	0.296±0.030 0.354±0.054	0.272±0.029 0.230±0.036	0.187±0.021 0.196±0.037

[a]Reference 49. [b]Reference 50.

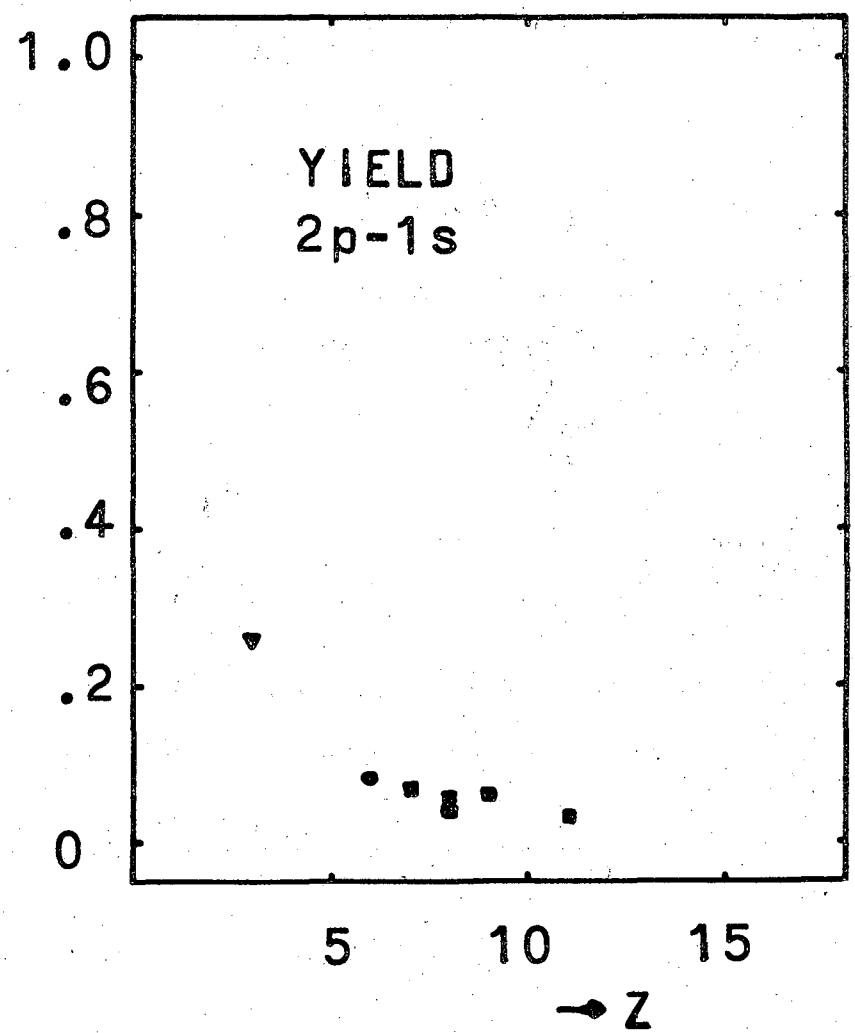

XBL 6812-6262

Fig. 13a. Pionic atom X-ray yields versus atomic number. Data plotted as circles are from Berkeley, crosses are from CERN, and triangles are from William and Mary.

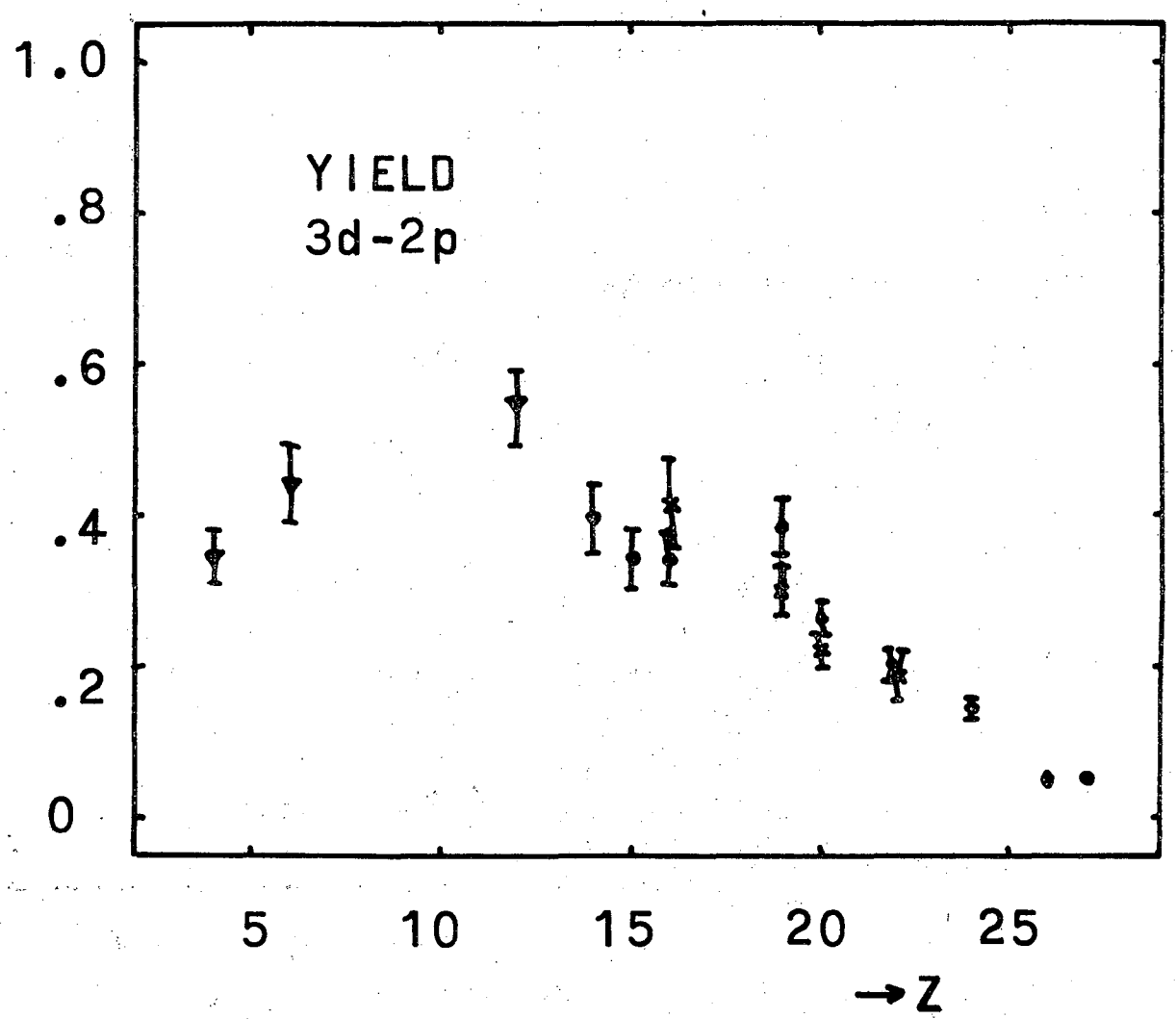

XBL 6812-6264

Fig. 13b. Pionic atom X-ray yields versus atomic number. Data shown as circles are from the earlier Berkeley measurements, crosses are from the recent Berkeley measurements, and trigangles are from William and Mary.

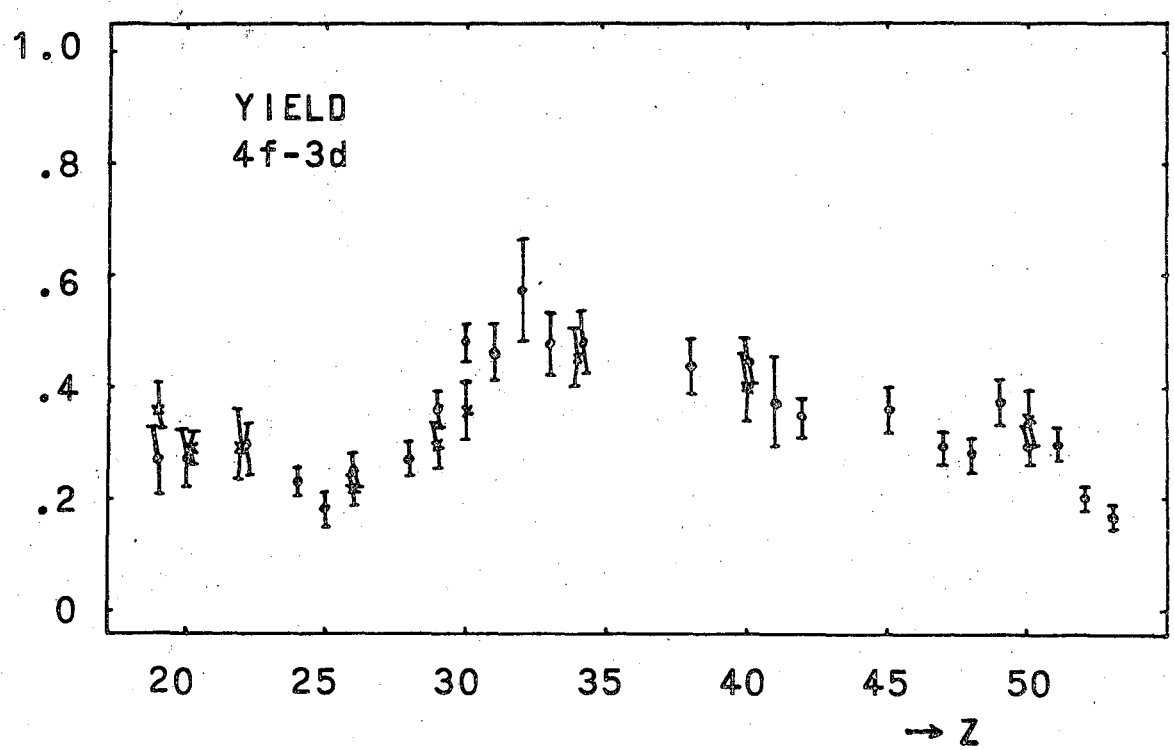

XBL 6812-6261

Fig. 13c. Pionic atom X-ray yields versus atomic number. Data plotted as circles are from the earlier Berkeley measurements and crosses are from the recent Berkeley measurements.

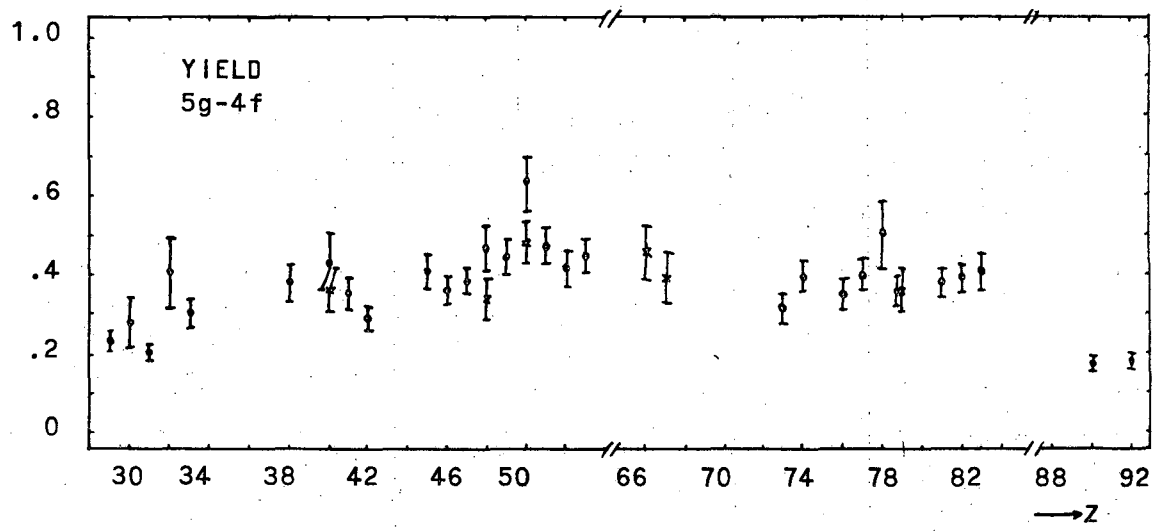

XBL 6812-6248

Fig. 13d. Pionic atom X-ray yields versus atomic number. Data plotted as circles are from earlier Berkeley measurements and crosses are from recent Berkeley measurements.

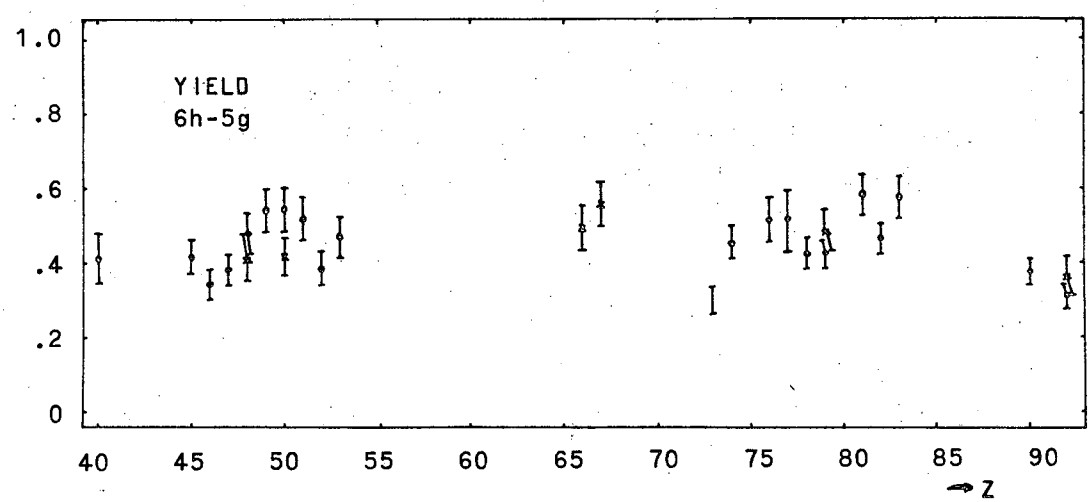

XBL 6812-6263

Fig. 13e. Pionic atom X-ray yields versus atomic number. Data plotted as circles are from the earlier Berkeley measurements and crosses are from the recent Berkeley measurements.

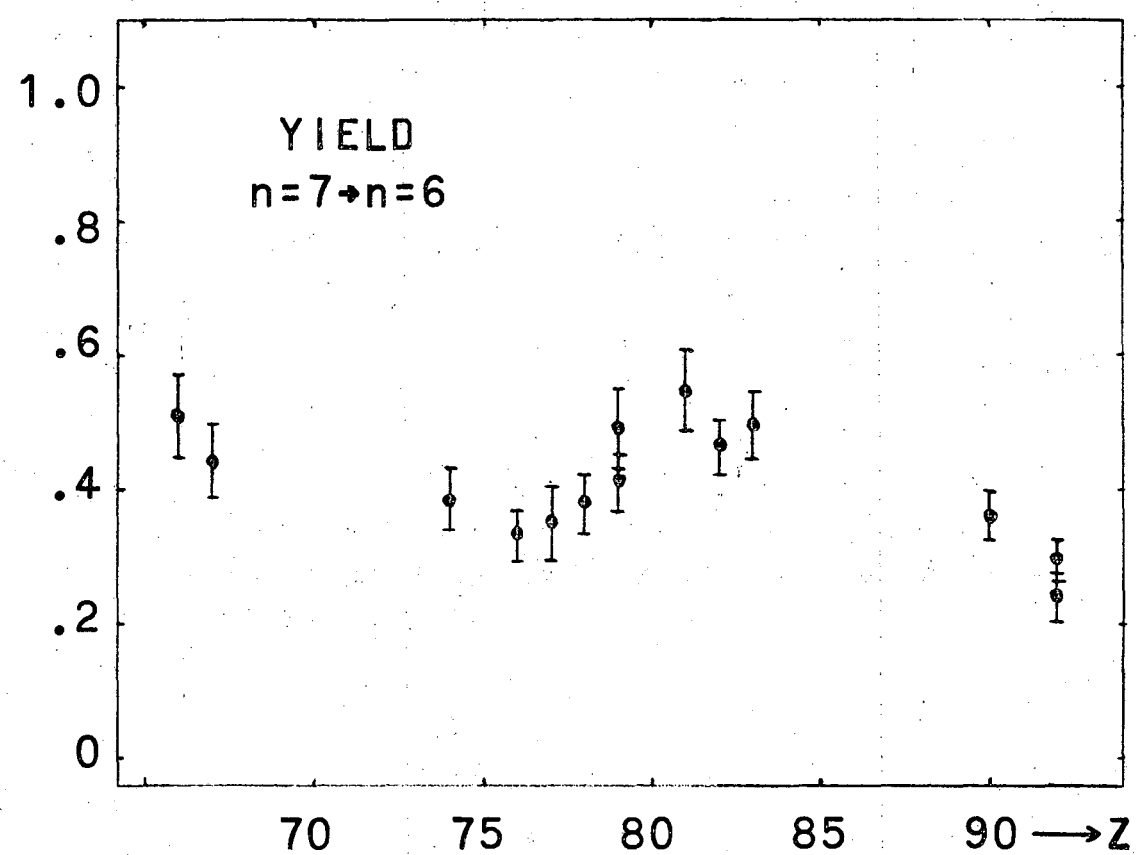

XBL 6812-6240

Fig. 13f. Pionic atom X-ray yields versus atomic number. Data plotted as circles are from the earlier Berkeley measurements and crosses are from the recent Berkeley measurements.

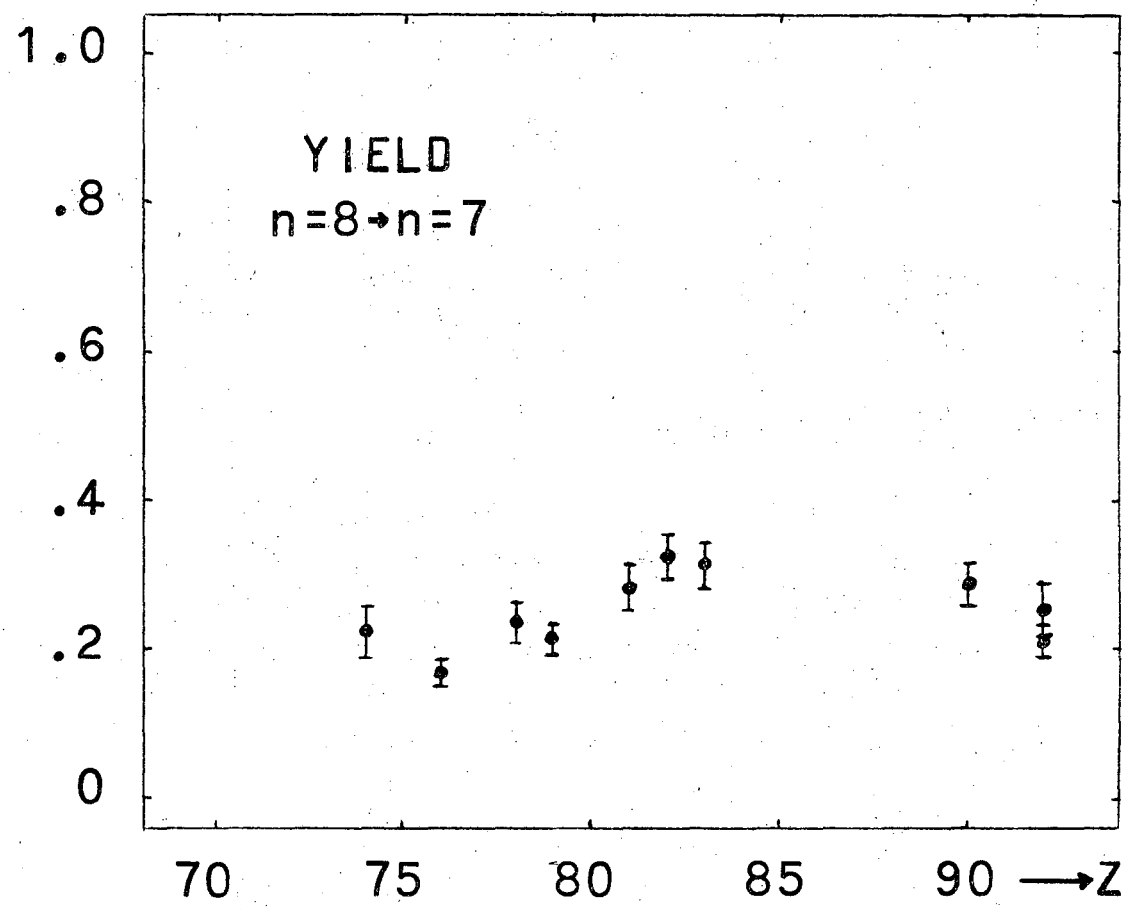

XBL 6812-6239

Fig. 13g. Pionic atom X-ray yields versus atomic number. Data plotted as circles are from the earlier Berkeley measurements and crosses are from the recent Berkeley measurements.

We obtain the Auger rates for the pion by considering the analogy to the internal conversion process.[52] The internal conversion coefficients represent the ratio of the number of electrons to the number of photons, internal conversion coefficient$=n_e/n_\gamma$. We find the coefficients[26,53] for Z-1 at the transition energy and multiply by the radiative rate to obtain the Auger rate:

$$R_a = \left(\frac{n_e}{n_\gamma}\right) R_{rt} \quad . \qquad \text{(IV-4)}$$

The mesic Auger process is also analogous to the photoelectric process.[54] The values obtained from calculations based on the photoelectric cross sections[27] agree in the region of interest with those from internal conversion. Figure 14 shows both the Auger and the radiative rates.

We find the nuclear capture rates from the strong interaction widths Γ by dividing by $\hbar$,

$$R_n = \frac{\Gamma}{\hbar} \quad . \qquad \text{(IV-5)}$$

We combine the three rates for the processes of radiation, Auger emission, and nuclear capture to calculate the radiative fraction of pions that leave the level $n_1\ell_1$ and go to level $n_2\ell_2$

$$\frac{R_r}{R_{rt}+R_a+R_n} \quad .$$

This fraction multiplied by the level population P, the probability of a captured pion reaching the level, is the radiative yield. The level population P is less than one due to other possible paths in the cascade and nuclear capture from low ℓ values. We assume that a constant level population is approximately correct as a function of Z. A least squares fit to the data gives the level population P for each

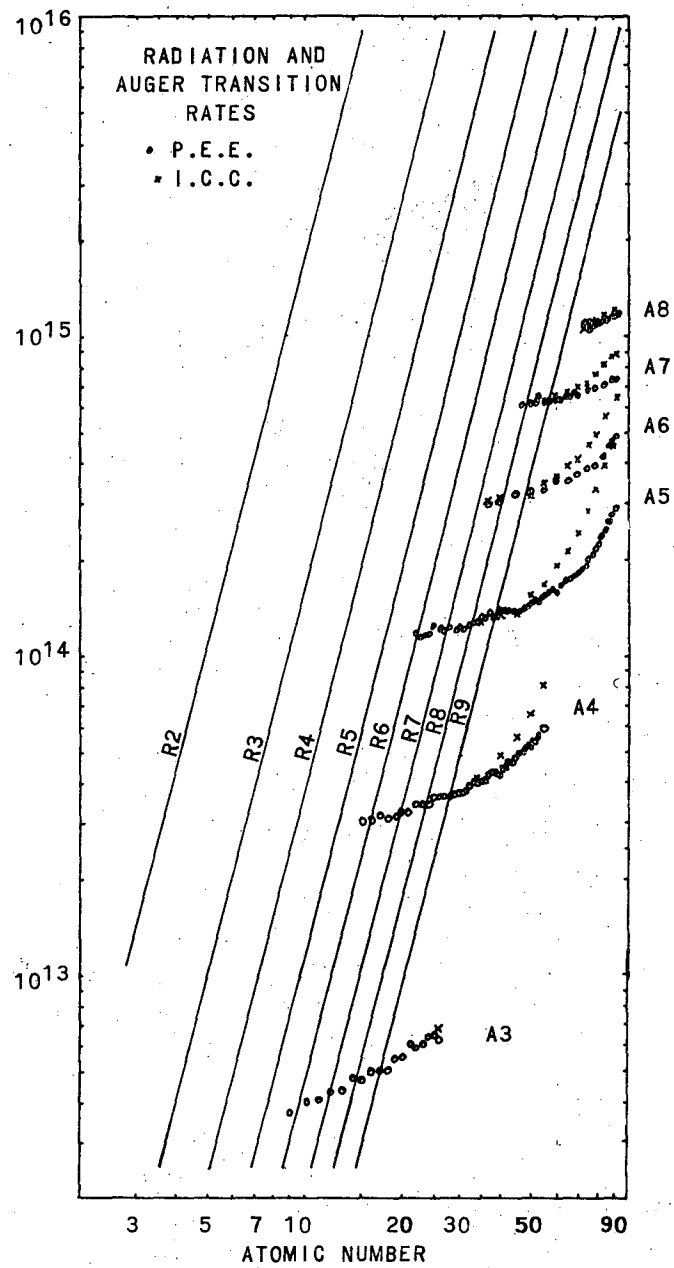

XBL 6812-6252

Fig. 14. Pionic atom Auger and radiative transition rates versus atomic number. The label Rn refers to the n → n-1 transition and the label An refers to the Auger rate from the n level. The text explains how the rates are found. A2 is much smaller than R2 and is out of the figure.

n (where the line is for $n \rightarrow n-1$ Table III lists the values of the level populations as determined by the fit.

We assume the level of a radiative transition to be the level of highest ℓ value for that particular n value (ℓ=n-1, circular Bohr orbits), even though several transitions may have nearly the same energy. This assumption is plausible by the following considerations of a specific example of $n_1=3$ going to $n_2=2$ for Z=20. The calculated radiative rates are as follows:

$$RR(3d\text{-}2p) = 2.80 \times 10^{15}\ sec^{-1}$$

$$RR(3p\text{-}2s) = 0.96 \times 10^{15}\ sec^{-1}$$

$$RR(3s\text{-}2p) = 0.28 \times 10^{15}\ sec^{-1}\ .$$

The Auger rates for these n=3 cases are small and about equal to $5 \times 10^{12}\ sec^{-1}$, hence are negligible.

We calculate the nuclear capture rates of the pion from the various levels by scaling the measured 1s, 2p, 3d rates for given ℓ values by the n dependence (found from $\int \rho\psi^2 dv$). They are approximately as follows:

$$RN(1s) = 4 \times 10^{20}\ sec^{-1}$$

$$RN(2s) = 5 \times 10^{18}\ sec^{-1}$$

$$RN(3s) = 1 \times 10^{16}\ sec^{-1}$$

$$RN(2p) = 3 \times 10^{18}\ sec^{-1}$$

$$RN(3p) = 8 \times 10^{15}\ sec^{-1}$$

$$RN(3d) = 2 \times 10^{15}\ sec^{-1}\ .$$

For the lower n values the s levels are completely captured. The 3p-2s transition X rays would be extremely shifted and broadened in comparison to the 3d-2p transition X rays. The state population will

Table III. Level populations P in mesonic atoms as a fraction of total mesons reaching the level.

Level	Experimental level populations from pion data[a]	Level populations calculated for muons for comparison only[b]	
		carbon	silicon
2p	0.57 ± 0.12	0.48	0.61
3d	0.36 ± 0.07	0.31	0.37
4f	0.38 ± 0.07	0.29	0.31
5g	0.34 ± 0.07	0.27	0.29
6h	0.45 ± 0.09	0.26	0.27
7i	0.41 ± 0.08	0.25	0.26
8j	0.30 ± 0.06	0.24	0.25

a. We used the values A_1=0.031 (λ^4) and A_2=0.171 (λ^6) in the formula (IV-5) to make the calculations.

b. From Reference 55.

favor the 3d over the 3p and 3s levels because a statistical population in n=14 is about correct and the nucleus will capture the lower ℓ values. The 3s-2p transition will not exist. The 3p-2s X rays will be less numerous than the 3d-2p X rays because all the effects tend to make its radiative yield lower: population of 3p is less than 3d, nuclear absorption of 3p is greater than 3d, and the radiative rate of 3d-2p is greater than 3p-2s.

The result of these effects is that for $n_1=3 \rightarrow n_2=2$ the predominant transition is 3d-2p. The same considerations apply to all other cases where nuclear absorption exists. Where nuclear absorption does not exist as an influence on the radiative yield, (eg. 8j-7i, 7i-6h) only the higher state populations and higher radiative rates favor the transitions of largest ℓ values.

No prediction for the level populations of pionic atoms exists. Eisenberg and Kessler[55] give level populations for muonic atoms but muons do not have the nuclear capture of the pions. They assume an initial distribution in the n=14 level where each of the levels denoted by the quantum number ℓ has a population of $2\ell+1$ mesons. Assuming the rates of the radiation and Auger electron emission known, they calculate the muon cascade to the various levels. Table III lists these level populations for carbon and silicon only for a comparison to the measured pion level populations. The fitting procedure includes the nuclear capture so that the pion values should agree with the muon values if no differences in the cascade exist. In conclusion the agreement is not satisfactory but the assumptions put into the two sets of numbers are considerable.

V. LINE INTENSITIES IN COMPOUNDS

A. Chemical Effects

X-ray intensities of lines in a spectrum demonstrate chemical effects in muonic atoms[17,18,19,20] and this has also been noted recently in pionic atoms.[21] The intensities differ if the element under consideration is pure or a part of a compound and, in particular, the ratios of line intensities differ.[18,19,20,21] Apart from this result, the so-called Fermi-Teller Z-law[56] appears valid only as a general and approximate rule (the prediction of capture on the constiutents of a compound in proportion to their atomic number). The nature of the chemical bond[17] appears to be a factor influencing the atomic capture ratio.

It seemed interesting to us to use the favorable π^- intensity available at the Berkeley 184-inch cyclotron to further study such effects. The use of π^- rather than μ^-, apart from the superior intensity, has some drawbacks. The nuclear capture perturbs the lower (deeper) transitions to a point where the 2p-1s, 3d-2p, and in high Z nuclei even 4f-3d X-ray transitions become difficult to observe or cannot be measured. However, for high enough orbits, in particular where the atomic capture takes place, the behavior should be the same for π^- and μ^-. This is again apart from the nuclear capture, which may affect non-circular low-ℓ orbits for pions (3s and 6d for example). We used the conventional method of producing and identifying stopped π^- as explained previously. The targets were usually discs of 7.5 cm diameter and 1.25 to 2.0 cm thick (1.5 - 3.5 gm/cm^2). We required a fast coincidence (~100ns) between the stopped pion signal (counters $12\bar{C}34$) and the fast output of the Ge amplifier system.[23] A pulse-

height analyzer recorded the coincident pulse-height spectrum from the slow Ge amplifier output. The fast coincidence caused no loss of good events above 50 keV while appreciably reducing (by 50%) the background due to chance coincidences. Each measurement lasted a few hours.

We scanned the spectra and evaluated the peak areas after subtracting the background. We used and cross-checked two methods. The first was a hand-and-eye method and the second and on-line computer fitting procedure. We corrected the data for the self-absorption of the X rays in the target and for the efficiency of the detector.

We measured an X-ray spectrum for a particular compound and also for the mixture of the same atomic ratio. Table IV displays the results. We calculated several types of line intensity ratios, either for lines associated with the same element in a compound or not, or for pairs of lines, one from each element of a compound or mixture. The errors include uncertainties in the background subtraction, in the detector efficiency, and in the target attenuation factor. When making a ratio of the ratios for a compound and mixture pair, the uncertainties on the efficiency and the attenuation factors canel or are reduced. Table IV reflects this reduction in uncertainty in the last column. In every case where it was necessary a correction took into account the differences in the yields of the elements, particularly because of nuclear capture of the pions. It was difficult to determine an absolute yield with an overall uncertainty smaller than ±10%, mainly from the evaluation of the true number of stopped π^-; but, the relative yields are known better, to ±5%. We measured these absolute yields

using the elements as targets whenever possible.

Before discussing the results we wish to emphasize that the ratio of capture on the two constituents of a compound can only be indirectly deduced from a measurement of two X-ray line intensities. The intensity covers two effects, one the initial atomic capture itself, and the other the subsequent process of the cascade. Several measurements[18-21] as well as these show that the cascades differ for a pure element and for the element in a compound. See especially the sets of numbers in Table IV for C, CH_2.

What is noticeable at first is that the capture ratio of the two elements of a compound usually differs from the same ratio in the mixture. However, a compound and the corresponding mixture should not be compared directly because the mixture could not be on the atomic level. The grain size for all constituents of the mixtures was smaller than 100 mesh (0.149mm) except for the Te which was 65 mesh (0.210mm) and they were much larger than the atomic size. For these mixtures, much larger than atomic size, the ratio of the macroscopic volumes as well as the ratio of the rate of energy loss will be effective. Using the densities of the elements in the mixtures and assuming as a first approximation that the rate of energy loss is proportional to Z, one can roughly explain the measured ratios for the mixtures.

A second effect which shows up is that of the chemical binding on the intensity ratios within each element of a compound. This supports the previous observations done with μ^-, in particular for the cases of Ti/TiO_2[18,19,20] and C/CH_2.[20] The effect, if any, for Ti is much smaller in our case, in agreement with Reference 21, possibly

because it was only possible to study the Paschen series with π^-. The effect for C is in agreement with the previous μ^- results; it is large and opposite to the Ti case, and probably a result of the H to C transfer of mesons. Transitions between circular orbits (i.e. with $\Delta\ell=1$, $\Delta n=1$), appear to be slightly favored in the compounds (see for example Ti/TiO_2, CdTe/Cd+Te, InSb/In+Sb).

Au-Yang and Cohen[57] studied this problem and showed that the capture takes place on high common molecular orbits and that chemical effects cannot be neglected. They performed numerical calculations for a few cases; in particular for ZnS they calculated a ratio of 3.0 which compares well with our experiment. In agreement, we found the atomic capture was influenced by the Z ratio, the ratio of the radii of the two types of ions or atoms and the effective charge transfer Z_f. The effective charge transfer characterizes the chemical bond. The definition of effective charge transfer is the amount of ionic character times the number of valence electrons where these parameters are from Pauling.[58] The ionic character of a bond A-B is related to the difference in electronegativity x_A-x_B of the atoms. The electronegativity scale is shown in Pauling. For $Z_1/Z_2 \leq 1$, Z_f may be the most important factor as in the case of ZnSe where the deviation of the Z-law is large. Figure 15 shows an example of a spectrum of a mixture and compound. The effect of Z_f, in favor of the positive ion, is perhaps small when $Z_1/Z_2 > 1$; it can also be counterbalanced by the effect of the ratio of the radii, usually smaller than one, favoring the negative ion. The comparison of FeS to FeS_2 is direct evidence of the effect of

Z_f.

The KCl and $CaCl_2$ solutions in water compared together and with the anhydrous salts also show the effect of Z_f, but with the complication brought by the disassociation. Concerning the Cu_3Au alloy, from the most reliable ratio, 4f-3d Cu/7i-6h Au, one might conclude that the unordered sample is closer to the mixture 3Cu+Au than the ordered sample. The electrical conductivity increased by a factor of two for the ordered sample after the thermal ordering process.

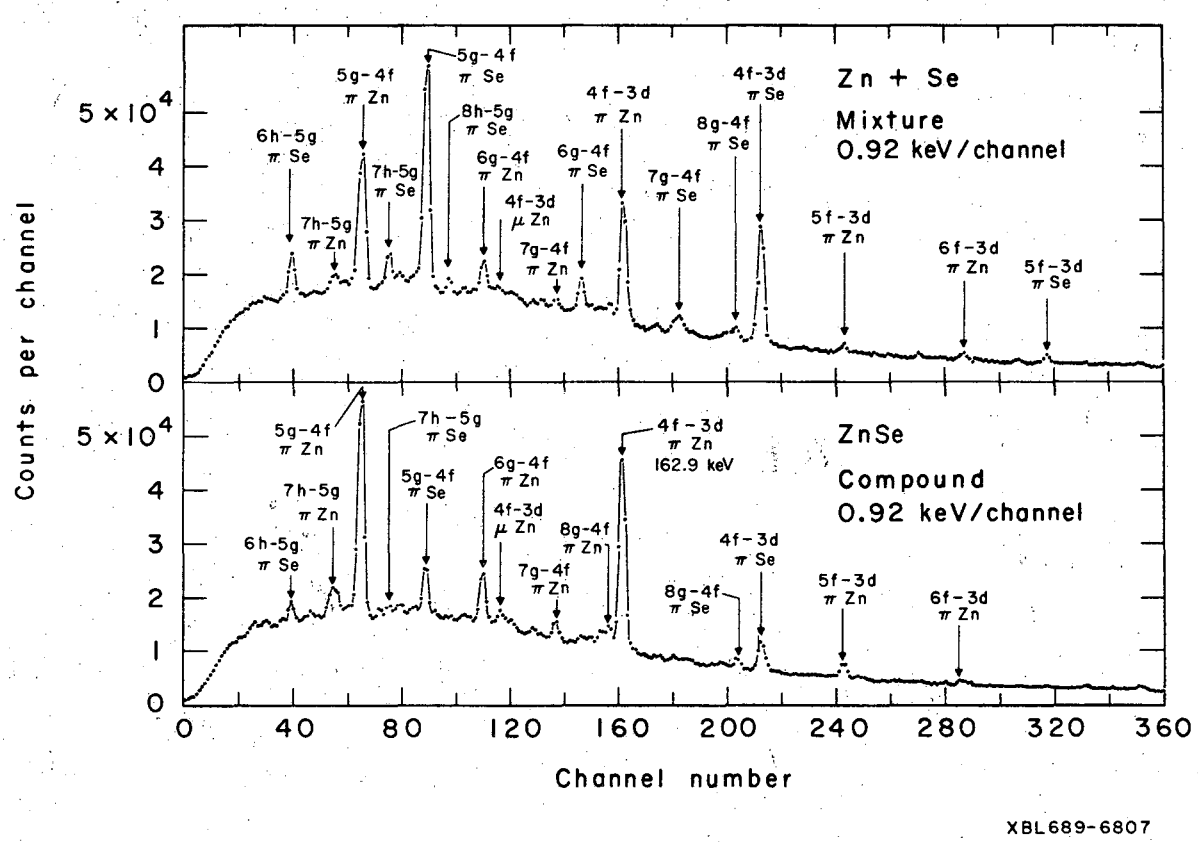

Fig. 15. Pionic atom X-ray spectrum of a compound and a mixture.

Table IV. Experimental results

The $CaCl_2$ and FeS_2 ratios are given for a one-to-one compound. The ratios given on the same lines as element yields include the effect of the latter.

Samples	Z_1/Z_2	Z_f[a]	Line ratio[b]	In first sample	In second sample	First line yield[c]	Second line yield[d]	Ratio of ratios[e]
ZnS, Zn+S	1.87	0.36	4f-3d Zn/3d-2p S	2.68 ±0.12	1.42 ±0.06			1.89 ±0.08
				2.54 ±0.31	1.35 ±0.17	0.40 ±0.05	0.38 ±0.04	
			5f-3d Zn/4f-3d Zn	0.16 ±0.01	0.130±0.007			1.23 ±0.08
			6g-4f Zn/5g-4f Zn	0.180±0.015	0.22 ±0.02			0.82 ±0.04
			4d-2p S/3d-2p S	0.145±0.012	0.175±0.015			0.83 ±0.09
ZnSe, Zn+Se	0.89	0.30	4f-3d Zn/4f-3d Se	3.57 ±0.19	0.64 ±0.04			5.58 ±0.34
				4.10 ±0.49	0.74 ±0.09	0.40 ±0.05	0.46 ±0.04	
			5f-3d Zn/4f-3d Zn	0.14 ±0.01	0.12 ±0.01			1.17 ±0.12
			6g-4f Zn/5g-4f Zn	0.14 ±0.01	0.18 ±0.02			0.78 ±0.07
FeS, Fe+S	1.62	0.24	4f-3d Fe/3d-2p S	1.67 ±0.10	0.74 ±0.04			2.26 ±0.11
				2.75 ±0.31	1.22 ±0.13	0.23 ±0.02	0.38 ±0.04	
FeS_2, Fe+2S	1.62	0.12	4f-3d Fe/3d-2p S	1.30 ±0.08	0.85 ±0.05			1.53 ±0.10
				2.15 ±0.24	1.40 ±0.16	0.23 ±0.02	0.38 ±0.04	
CdTe, Cd+Te	0.92	0.08	5g-4f Cd/5g-4f Te	0.84 ±0.05	0.77 ±0.05			1.09 ±0.07
				0.90 ±0.10	0.82 ±0.09	0.40 ±0.04	0.43 ±0.04	
			6h-5g Cd/6h-5g Te	0.83 ±0.08	0.72 ±0.07			1.15 ±0.10
				0.85 ±0.11	0.74 ±0.10	0.44 ±0.04	0.45 ±0.04	
			7h-5g Cd/6h-5g Cd	0.230±0.025	0.25 ±0.03			0.92 ±0.11
			7h-5g Te/6h-5g Te	0.155±0.02	0.18 ±0.02			0.86 ±0.13
			7i-6h Te/6h-5g Te	1.18 ±0.12	0.85 ±0.10			1.39 ±0.16
InSb, In+Sb	0.96	0.03	5g-4f In/5g-4f Sb	1.02 ±0.05	0.99 ±0.05			1.03 ±0.05
				1.07 ±0.11	1.04 ±0.10	0.43 ±0.04	0.45 ±0.04	
			6h-5g In/6h-5g Sb	0.94 ±0.09	0.91 ±0.09			1.03 ±0.09
				0.94 ±0.12	0.91 ±0.12	0.47 ±0.04	0.47 ±0.04	
			7h-5g In/6h-5g In	0.195±0.025	0.23 ±0.03			0.85 ±0.13
			7h-5g Sb/6h-5g Sb	0.21 ±0.02	0.225±0.030			0.93 ±0.14
Ti, TiO_2			5f-3d Ti/4f-3d Ti	0.208±0.018	0.200±0.018			1.04 ±0.08
			6f-3d Ti/4f-3d Ti	0.214±0.020	0.207±0.020			1.04 ±0.09
			7f-3d Ti/4f-3d Ti	0.049±0.006	0.059±0.008			0.84 ±0.14
			7g-4f Ti/4f-3d Ti	0.157±0.019	0.147±0.018			1.07 ±0.12
			4f-3d Ti/3d-2p Ti	1.59 ±0.14	1.59 ±0.15			1.00 ±0.14
				1.05 ±0.14	1.05 ±0.15	0.295±0.03	0.195±0.02	
C, CH_2			3p-1s C/2p-1s C	0.21 ±0.03	0.29 ±0.04			0.71 ±0.11
			4p-1s C/2p-1s C	0.135±0.025	0.215±0.03			0.63 ±0.12
			5p-1s C/2p-1s C	0.11 ±0.02	0.245±0.035			0.45 ±0.09
$CaCl_2$,$CaCl_2(H_2O)$	1.18	0.62	3d-2p Ca/3d-2p Cl	0.775±0.040	0.82 ±0.05			0.95 ±0.06
				1.15 ±0.12	1.22 ±0.12	0.24 ±0.02	0.355±0.03	
			5f-3d Ca/3d-2p Cl	1.44 ±0.12	1.40 ±0.23			1.03 ±0.17
			6f-3d Ca/5f-3d Ca	0.46 ±0.05	0.35 ±0.12			1.30 ±0.45
			4d-2p Cl/3d-2p Cl	0.09 ±0.01	0.12 ±0.02			0.74 ±0.14
KCl, $KCl(H_2O)$	1.12	0.70	3d-2p K/3d-2p Cl	0.99 ±0.04	0.71 ±0.05			1.39 ±0.10
				1.13 ±0.11	0.81 ±0.94	0.31 ±0.03	0.355±0.03	
			4f-3d K/3d-2p Cl	1.15 ±0.07	0.91 ±0.07			1.27 ±0.07
				1.32 ±0.13	1.04 ±0.12	0.31 ±0.03	0.355±0.03	
CsCl	3.23	0.73	5g-4f Cs/3d-2p Cl	2.33 ±0.11				
				1.84 ±0.20		0.45 ±0.05	0.355±0.03	
			6h-5g Cs/3d-2p Cl	2.02 ±0.10				
				1.63 ±0.16		0.44 ±0.04	0.355±0.03	
			7h-5g Cs/6h-5g Cs	0.19 ±0.02				
$^{44}CaCl_2$, $^{40}CaCl_2$			3d-2p Ca/3d-2p Cl	0.835±0.055	0.89 ±0.06			0.94 ±0.08
				1.25 ±0.13	1.31 ±0.14	0.24 ±0.02	0.355±0.03	
			6f-3d Ca/6f-3d Cl	2.01 ±0.22	2.15 ±0.22			0.94 ±0.10
			4d-2p Cl/3d-2p Cl	0.115±0.010	0.125±0.010			0.93 ±0.10
			4f-3d Ca/3d-2p Cl	0.895±0.080	0.945±0.080			0.95 ±0.08
				1.11 ±0.14	1.18 ±0.15	0.285±0.025	0.355±0.03	
Cu_3Au(ordered),			4f-3d Cu/7i-6h Au	0.407±0.022	0.427±0.023			0.95 ±0.05
Cu_3Au(unordered)				0.670±0.065	0.702±0.068	0.31 ±0.03	0.46 ±0.03	
3Cu+Au			4f-3d Cu/7i-6h Au	0.442±0.027				
				0.726±0.074		0.31 ±0.03	0.46 ±0.03	

a. Effective charge transfer, defined in text.
b. The ratio of the intensity of the two listed transition lines.
c. Transition line yield in the first element of column 4 defined as number of X-rays per stopped pion.
d. Transition line yield in the second element of column 4 defined as number of X-rays per stopped pion.
e. Ratio of the intensity ratios of columns 5 and 6.

B. Chlorides

The process of interest for pionic atoms with chlorine chemical compounds is the initial atomic capture probability for the pion on the constituents of the compound. If there is a negligible amount of pion transfer between the constituents, the ratio of initial pion capture will be preserved during the cascade and measured by means of observable X-ray transitions. Observations show differences in the ratios of intensities between the pure element and the same element in a compound.[17-22] This result implies that a complete knowledge of the details of the cascade process is necessary to interpret data on radiative yields in chemical compounds.

We used binary chlorine compound targets and measured the counts in the peak of the chlorine 3d-2p lines and the observed lines of the other constituent. We combined these data on the elements in the chlorine compound with the yields of the elements alone to obtain the initial pion capture probability on the constituents of the compound. The element radiative yields came from the curves of Fig. 13 so that even though chlorine was not used as a target interpolation from the 3d-2p yields gave the yield of chlorine.

The yield of a transition line will be lower in the compound than in the element because the pions are shared between the constituents. The relation between the yield in the compound Y_c, the yield in the element Y_e, and the initial capture probability W_z is

$$Y_c = mW_z Y_e \quad , \qquad \text{(V-1)}$$

where m is the atomic concentration (in $CaCl_2$ m=1). A similar relation

holds for the chlorine part of the compound

$$Y_c' = n\, W_{Cl}\, Y_e' \quad , \qquad \text{(V-2)}$$

where W_{Cl} is the initial atomic capture probability on the chlorine in the compound, and n is the atomic concentration (in $CaCl_2$ n=2). Solving these two equations for the ratio of initial atomic capture probability gives

$$\frac{W_z}{W_{Cl}} = \frac{n}{m}\frac{Y_c}{Y_c'}\frac{Y_e'}{Y_e} \quad . \qquad \text{(V-3)}$$

Since one finds the two compound yields Y_c and Y_c' at the same time for the same target, the stopped pion scaler number will cancel and the yield ratios are only the counts in the peak divided by the target transmission and detector efficiency. Figure 16 shows the initial atomic capture ratios for pions along with initial atomic capture ratios for muons on halogen compounds.[17] Table V lists the data.

Table V. Initial meson capture on halogen compounds.

	Sample	Z_1/Z_2	n_i [a]	W_{z1}/W_{z2} [b]
Pions	$AlCl_3$	0.76	3	1.57 ± 0.24
	$BaCl_2$	3.30	6	2.00 ± 0.30
			5	2.40 ± 0.36
	$MnCl_2$	1.47	4	2.10 ± 0.32
	$FeCl_2$	1.53	4	1.99 ± 0.30
	$ZnCl_2$	1.77	4	1.69 ± 0.25
	$SrCl_2$	2.24	4	1.16 ± 0.17
	NaCl	0.65	3	0.87 ± 0.13
	$Ca^{40}Cl_2$	1.18	3	1.16 ± 0.12
	$Ca^{44}Cl_2$	1.18	3	1.25 ± 0.13
	NiCl	1.65	4	2.34 ± 0.35
	LiCl	0.18	2	0.18 ± 0.18
	CsCl	3.23	5	1.84 ± 0.20
			6	1.63 ± 0.16
	KCl	1.12	4	1.33 ± 0.13
			3	1.13 ± 0.11
Muons [c]	PbCl	4.82	2	3.16 ± 0.24
	NaCl	0.65	2	1.05 ± 0.08
	$CaCl_2$	1.18	2	1.56 ± 0.17
	KI	0.36	2	0.50 ± 0.05
	NaI	0.21	2	0.29 ± 0.03
	CdI	0.91	2	1.0 ± 0.2
	AgI	0.89	2	1.45 ± 0.25
	PbI_2	1.55	2	1.22 ± 0.11
	LiF	0.33	2	0.28 ± 0.03
	NaF	1.22	2	1.56 ± 0.12
	PbF_2	9.10	2	4.7 ± 0.4

a. Initial level of measured transition.

b. Ratio of capture on the two constituents Z_1 and Z_2.

c. Data from Reference 17.

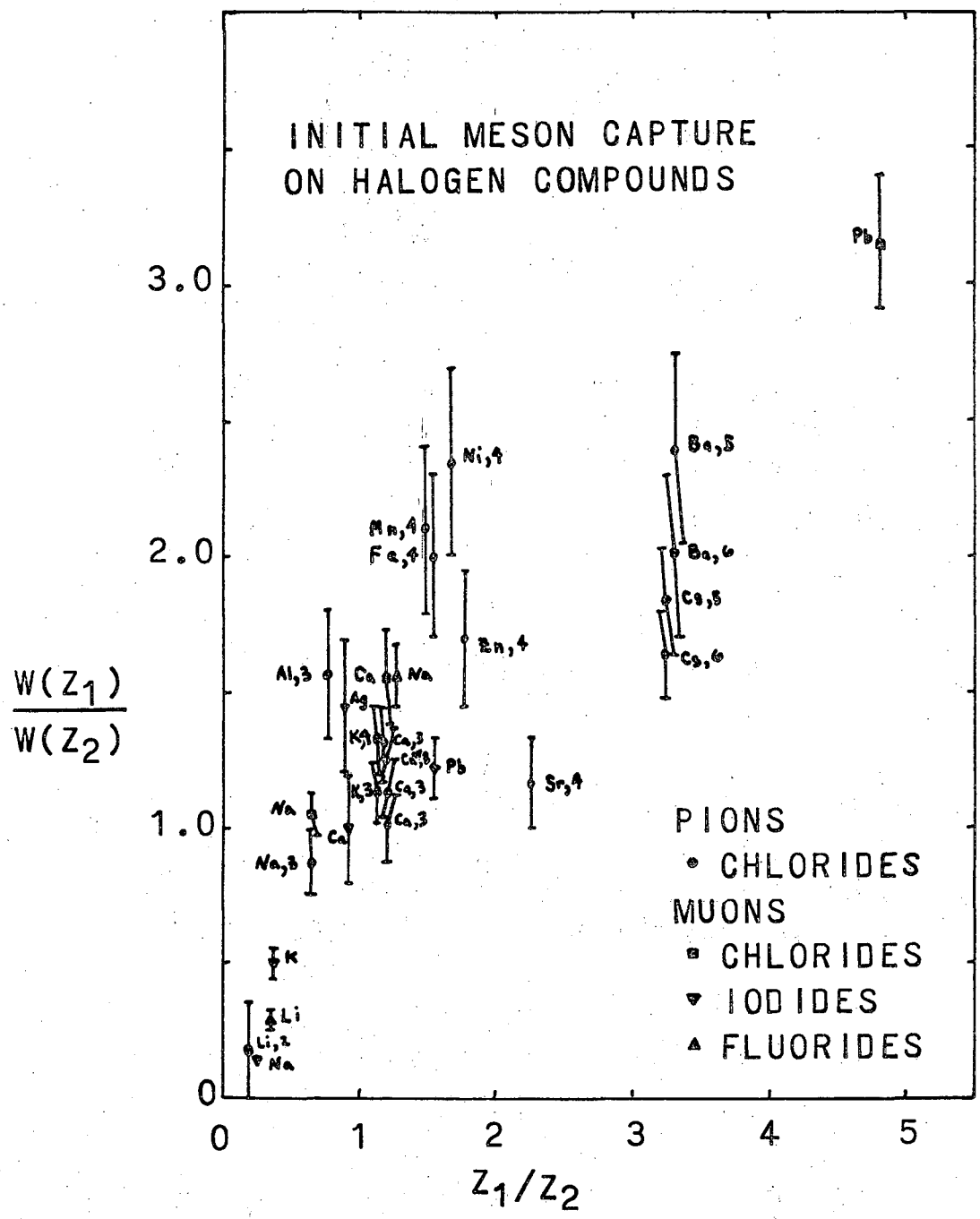

XBL 6812-6250

Fig. 16. Initial meson capture on halogen compounds. The value of n listed after the Z_1 constituent of a chloride is the initial level of the measured pion transition. All muon transitions are for n initial equal to 2.

ACKNOWLEDGMENTS

I thank Professor Emilio Segrè for his most valued advice and encouragement.

I thank Dr. G. A. Grin and Dr. D. A. Jenkins for their work on this experiment.

I thank Dr. K. Crowe and Dr. C. Wiegand for their interest in this work.

I thank for discussions and assistance Dr. N. Dairiki, Mr. T. Mottershead, Mr. P. Kijewski, and Dr. M. Chen.

I thank my wife Laurie for her assistance and patience.

I thank Mrs. Rosemary Fowell for her help in the typing.

APPENDIX

1. Radial hydrogen wave functions.

$$R_n = C_n\left(\frac{Z}{a}\right)^{\left(\frac{2n+1}{2}\right)} r^{(n-1)} e^{-\left(\frac{Zr}{na}\right)} ,$$

where

$$a = \frac{\hbar}{m_\pi e^2} = 193.73 \text{ fm} ,$$

$$C_n = \frac{2^n}{n^{n+1}\sqrt{(2n-1)!}} .$$

2. Overlap integrals for a uniform density nucleus.

Define

$$B = \frac{2Z}{na} ,$$

and

$$\rho_o(r) = \begin{cases} \rho_o & r < R \\ 0 & r > R \end{cases} ,$$

where R is the nuclear radius and

$$\rho_o = \frac{3A}{4\pi R^3} ,$$

$$\int \psi^2 \rho(r) dv = C_n^2 \left(\frac{Z}{a}\right)^{2n+1} \rho_o \int_o^R e^{-Br} r^{2n} dr$$

$$= C_n^2 \left(\frac{Z}{a}\right)^{2n+1} \rho_o \left[1 - e^{-BR}\left(1 + BR + \frac{(BR)^2}{2} + \dots + \frac{(BR)^{2n}}{(2n)!}\right)\right] \frac{(2n)!}{B^{2n+1}} .$$

$$\int |\nabla\psi|^2 \rho(r) dv = (n-1)(2n-1)C_n^2 \left(\frac{Z}{a}\right)^{2n+1} \rho_o \int_o^R r^{2n-2} e^{-Br} dr -$$

$$- 2\left(\frac{Z}{na}\right)(n-1)C_n^2\left(\frac{Z}{a}\right)^{2n+1} \rho_o \int_o^R r^{2n-1} e^{-Br} dr +$$

$$+ \left(\frac{Z}{na}\right)^2 C_n^2 \left(\frac{Z}{a}\right)^{2n+1} \rho_o \int_o^R r^{2n} e^{-Br} dr$$

$$= (n-1)(2n-1)F(2n-2) - 2\left(\frac{Z}{na}\right)(n-1)F(2n-1) +$$

$$+ \left(\frac{Z}{na}\right)^2 F(2n) ,$$

where

$$F(2n) = \int \psi^2 \rho(r) dv .$$

3. Derivation of natural line width formula

Measured line $\Gamma_m = B$

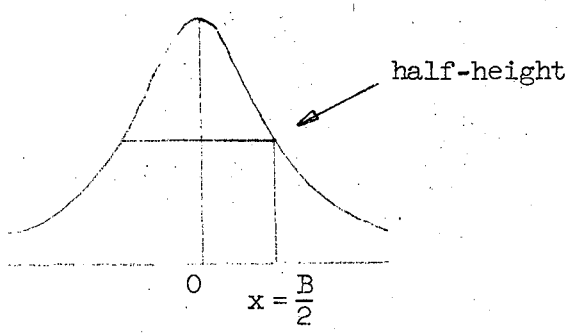

Instrumental line $\Gamma_i = 1.66\ G$

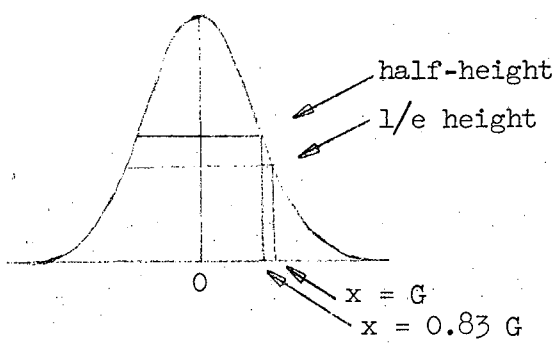

Natural line $\Gamma_n = 2D$

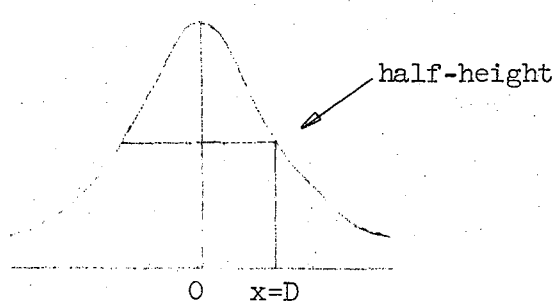

Using from Allen[28]

$$B^2 + D^2 - 2BD = D^2 + 2.80\ G^2 ,$$

we have for the relation of the full width at half maximum

$$\Gamma_m^2 - 2\,\frac{\Gamma_n}{2}\,\Gamma_m = 2.80\,\frac{\Gamma_i^{\,2}}{(1.67)^2} ,$$

or

$$\Gamma_n = \Gamma_m - \Gamma_i^{\,2}/\Gamma_m .$$

By the rules for the combination of experimental errors, we derive the error on the natural line width due to the errors on the instrumental line width and the measured line width.

$$\delta\Gamma_n = \frac{4\Gamma_i^{\,2}}{\Gamma_m^{\,2}}\,\delta\Gamma_i^{\,2} + \left(1 + \frac{2\Gamma_i^{\,2}}{\Gamma_m^{\,2}} + \frac{\Gamma_i^{\,4}}{\Gamma_m^{\,4}}\right)\delta\Gamma_m^{\,2} \quad .$$

REFERENCES

1. H. Yukawa, Proc. Phys.-Math. Soc. (Japan) 17, 48 (1935).

2. C. M. G. Lattes, H. Muirhead, G. P. S. Occhialini, and C. F. Powell, Nature 159, 694 (1947).

3. E. Fermi, E. Teller, and V. Weisskopf, Phys. Rev. 71, 314 (1947).

4. E. Fermi and E. Teller, Phys. Rev. 72, 399 (1947).

5. M. Camac, A. D. McGuire, J. B. Platt, and H. J. Schulte, Phys. Rev. 88, 134 (1952).

6. M. B. Stearns, M. Stearns, L. Leipuner, and S. DeBenedetti, Phys. Rev. 95, 625A (1954).

7. D. West, Repts. Prog. Phys. 21, 271 (1958).

8. R. E. Shafer, K. M. Crowe, and D. A. Jenkins, Phys. Rev. Letters 14, 923 (1965).

9. M. Ericson and T. E. O. Ericson, Ann. Phys. 36, 323 (1966).

10. D. A. Jenkins and K. M. Crowe, Phys. Rev. Letters 16, 637 (1966).

11. D. A. Jenkins, R. Kunselman, M. K. Simmons, and T. Yamazaki, Phys. Rev. Letters 17, 1 (1966).

12. D. A. Jenkins and R. Kunselman, Phys. Rev. Letters 17, 1148 (1966).

13. R. Kunselman and G. A. Grin, to be published.

14. G. Backenstoss, S. Charalambus, H. Daniel, H. Koch, G. Poelz, H. Schmitt, and L. Tauscher, Phys. Letters 25B, 365 (1967).

15. G. Poelz, H. Schmitt, L. Tauscher, G. Backenstoss, S. Charalambus, H. Daniel, and H. Koch, Phys. Letters 26B, 331 (1968).

16. R. J. Harris, Jr., W. B. Shuler, M. Eckhause, R. T. Siegel, and R. E. Welsh, Phys. Rev. Letters 20, 505 (1968).

17. V. G. Zinov, A. D. Konin, and A. J. Mukhin, J. Nucl. Phys. (U.S.S.R.) 2, 859 (1965); (translation: Soviet J. Nucl. Phys. 2, 613 (1965)).

18. V. G. Zinov, A. D. Konin, A. J. Mukhin, and R. V. Polyakova, J. Nucl. Phys. (U.S.S.R.) 5, 591 (1967); (translation: Soviet J. Nucl. Phys. 5, 420 (1967)).

19. D. Kessler, H. L. Anderson, M. S. Dixit, H. J. Evans, R. J. McKee, C. K. Hargrove, R. D. Barton, E. P. Hincks, and J. D. McAndrew, Phys. Rev. Letters 18, 1179 (1967).

20. H. Daniel, H. Koch, G. Poelz, H. Schmitt, L. Tauscher, G. Backenstoss, and S. Charalambus, Phys. Letters 26B, 281 (1968).

21. L. Tauscher, G. Backenstoss, S. Charalambus, H. Daniel, H. Koch, G. Poelz, and H. Schmitt, Phys. Letters 27A, 581 (1968).

22. R. Kunselman and G. A. Grin, to be published.

23. F. S. Goulding, D. A. Landis, and R. H. Pehl, UCRL-17560 (submitted to Gatlinburg Conference on Semi-Conductor Detectors and Associated Circuits, May 1967).

24. International Atomic Energy Agency Vienna; Sets No. 95 and 130 containing ^{241}Am, ^{57}Co, ^{203}Hg, ^{22}Na, ^{137}Cs, and ^{60}Co.

25. C. M. Lederer, J. M. Hollander, and I. Perlman, Table of Isotopes, Sixth Edition, John Wiley and Sons, Inc., New York (1967).

26. K. Siegbahn, Alpha-, Beta- and Gamma-Ray Spectroscopy, North-Holland Publishing Co., Amsterdam, (1965).

27. E. Storm, E. Gilbert, and H. Israel, Los Alamos report LA-2237

28. M. Ciafaloni, Nuovo Cimento 52A, 274 (1967).

29. A. B. Mickelwait and H. C. Corben, Phys. Rev. 96, 1145 (1954). A. B. Mickelwait, thesis, Carnegie Mellon Institute, (1954) (unpublished).

30. G. E. Pustovalov, Zh. Eksperim. i Teor. Fiz. (U.S.S.R.) 36, 1806 (1959); English translation: Soviet Phys.-JETP 36, 1288 (1959).

31. C. W. Allen, Astrophysical Quantities, The Athlone Press, The University of London, London, England, 2nd Edition, p. 82 (1963).

32. A. Astbury, J. P. Deutsch, K. M. Crowe, R. E. Shafer, and R. E. Taylor, Comptes Rendus du Congrès International de Physique Nucleaire, Paris, 1964, ed. by P. Gugenberger (Centre National de la Recherche Scientifique, Paris, 1964), Vol. 2, p. 225.

33. J. Wetmore, D. C. Buckle, J. R. Kane, and R. T. Siegel, Phys. Rev. Letters 19, 1003 (1967).

34. G. H. Miller, M. Eckhause, W. W. Sapp, and R. E. Welsh, W. and M.-14, submitted for publication.

35. L. Suelzle, M. Yearian, and H. Crannell, Phys. Rev. 162, 992 (1967).

36. U. Meyer-Berkhout, K. W. Ford, and A. E. S. Green, Ann. Phys. 8, 119 (1959).

37. T. Stovall, J. Goldemberg, and D. Isabelle, Nucl. Phys. 86, 225 (1966).

38. R. Herman and R. Hofstadter, High Energy Electron Scattering Tables, Stanford University Press, Stanford, 1960.

39. H. Daniel, G. Poelz, H. Schmitt, G. Backenstoss, H. Koch, and S. Charalambus, Zeit. für Physik, 205, 472 (1967).

40. K. J. van Oostrum, R. Hofstadter, G. K. Nöldeke, M. R. Yearian, B. C. Clark, R. Herman, and D. G. Ravenhall, Phys. Rev. Letters 16, 528 (1966).

41. J. Orear, Notes on Statistics for Physicists, UCRL-8417 (unpublished) (1958).

42. A. Partensky and M. Ericson, Nuclear Physics B1, 382 (1967).

43. M. Ericson, Comp. Rend. 258, 1471 (1964).

44. C. Lovelace, CERN-TH839 (1967). (Invited paper at the Conference on πN Scattering held at the Univ. of Calif., Irvine, Dec. 1967)

45. J. Hamilton and W. S. Woolcock, Rev. Mod. Phys. 35, 737 (1963).

46. C. M. Rose, Jr., Phys. Rev. 154, 1305 (1967).

47. R. J. Harris, Jr., thesis, College of William and Mary (1968) (unpublished).

48. R. Seki and A. H. Cromer, Phys. Rev. 156, 93 (1967).

49. W. W. Sapp, College of William and Mary, private communication.

50. H. Koch, G. Poelz, H. Schmitt, L. Tauscher, G. Backenstoss, S. Charalambus, and H. Daniel, submitted to Phys. Letters.

51. L. Green, P. Rush, and C. Chandler, Astrophysical J. Supp. Ser. 3, 37 (1957).

52. E. H. S. Burhop, The Auger Effect, Cambridge, University Press, 1952.

53. M. Rose, Internal Conversion Coefficients, North-Holland Pub. Co., Amsterdam, 1958.

54. R. A. Ferrell, Phys. Rev. Letters 4, 425 (1960).

55. Y. Eisenberg and D. Kessler, Nuovo Cimento 19, 1195 (1961).

56. D. Fermi and E. Teller, Phys. Rev. 72, 399 (1947).

57. M. Y. Au-Yang and M. L. Cohen, Phys. Rev. (to be published).

58. L. Pauling, The Nature of the Chemical Bond, 3rd edition, Cornell University Press, 1960, Ithaca, New York.

LEGAL NOTICE

This report was prepared as an account of Government sponsored work. Neither the United States, nor the Commission, nor any person acting on behalf of the Commission:

A. Makes any warranty or representation, expressed or implied, with respect to the accuracy, completeness, or usefulness of the information contained in this report, or that the use of any information, apparatus, method, or process disclosed in this report may not infringe privately owned rights; or

B. Assumes any liabilities with respect to the use of, or for damages resulting from the use of any information, apparatus, method, or process disclosed in this report.

As used in the above, "person acting on behalf of the Commission" includes any employee or contractor of the Commission, or employee of such contractor, to the extent that such employee or contractor of the Commission, or employee of such contractor prepares, disseminates, or provides access to, any information pursuant to his employment or contract with the Commission, or his employment with such contractor.

TECHNICAL INFORMATION DIVISION
LAWRENCE RADIATION LABORATORY
UNIVERSITY OF CALIFORNIA
BERKELEY, CALIFORNIA 94720